Design of an Aluminum-Powered Reverse Osmosis Desalination System for Disaster Relief

by

Peter Godart

Submitted to the Department of Mechanical Engineering
in partial fulfillment of the requirements for the degree of

Master of Science in Mechanical Engineering

at the

MASSACHUSETTS INSTITUTE OF TECHNOLOGY

June 2019

© Massachusetts Institute of Technology 2019. All rights reserved.

Signature redacted

Author .....
Department of Mechanical Engineering
May 22, 2019

Signature redacted

Certified by .....
Douglas P. Hart
Professor
Thesis Supervisor

Signature redacted

Accepted by .....
Nicolas Hadjiconstantinou
Chairman, Department Committee on Graduate Theses

MASSACHUSETTS INSTITUTE OF TECHNOLOGY
JUN 13 2019
LIBRARIES
ARCHIVES

Design of an Aluminum-Powered Reverse Osmosis Desalination System for Disaster Relief

by

Peter Godart

Submitted to the Department of Mechanical Engineering
on May 22, 2019, in partial fulfillment of the
requirements for the degree of
Master of Science in Mechanical Engineering

Abstract

Fuel generated from highly energy-dense aluminum debris (23.3 kWh/L) is explored here as a means for producing electricity and clean water for disaster relief and preparedness. Energy is extracted from aluminum by first treating it with a minimal surface coating of gallium and indium (<3% by mass) and then reacting it with water to produce hydrogen, which can supply a fuel cell or internal combustion engine to generate electricity, and heat, which can be used to desalinate and purify seawater or contaminated fresh water.

To use aluminum debris as fuel, it is necessary to first understand which of the many possible aluminum-water reactions occurs at given a temperature and pressure in order to accurately model such quantities as the heat released and the amount of water required stoichiometrically for the reaction to proceed. A new thermodynamics analysis is presented here that predicts these quantities by minimizing the Gibbs free energy over the possible reactions to determine which is most favorable under a wide range operating conditions. Reaction experiments at the extremities of this range validate these results.

This new aluminum-water reaction model enables the design of a robust and minimally complex system that uses the heat released in this reaction to desalinate seawater. The system presented here uses a novel process called Heat-Driven Reverse Osmosis (HDRO), in which the release of thermal energy in an enclosed vessel pressurizes a working fluid up the high pressures required to drive reverse osmosis. Using the aluminum-water reaction as the heat source for this process, the theoretical upper limit performance ratio is shown to be 41 for 3.5% salinity seawater and maximum operating pressure of 138 bar, and an unoptimized prototype has achieved a performance ratio of 3. Additionally, because the hydrogen produced in the aluminum-water reaction is not consumed in this process, it can be used to generate electricity or desalinate additional water, further increasing the system-wide efficiency. Thus, in addition to being well-suited for disaster relief, this technology is a potentially attractive option for large-scale desalination in drought prone regions as well.

Thesis Supervisor: Douglas P. Hart
Title: Professor

Acknowledgments

This work came together with the help of numerous colleagues, sponsors, mentors, friends, and family members, whom I have been extremely grateful for throughout this process. First, to my parents, after all these years, I still do not regret you pushing me to apply for and attend MIT as an undergrad. Your interest in and willingness to contribute to my work has been extremely encouraging. Thank you for your support, and I am looking forward to what the future brings us.

To my grandmother, thank you for enduring all that you had to in order to make to and in this country to pave the way for us to succeed. Your unwavering support and (sometimes unsolicited) wisdom since day one have been a key part of making me who I am today and I cannot thank you enough.

To Tiandra, I am forever grateful for you putting up with me during quals and the ensuing madness. You handle all situations with incredible grace and integrity, and I genuinely aspire to be on your level of humanity some day.

To my friends in music and *beyond*, thank you for helping me stay grounded and generally for being the most generous, loving, and incredibly interesting people I know. Life is not worth living without you.

To my mentors, Fred, John and Rosie, Ran, and Gloria, your guidance and love has enabled me to keep a healthy mix of music at the forefront of my life, and have been largely responsible for helping maintain my sanity throughout this entire journey. Thank you.

To Doug, you have helped stoke my entrepreneurial drive, given me incredible space and support for me to explore my passions for research and teaching, and most importantly, you continuously remind me to not take myself too seriously. Looking forward to continuing this work with you and whatever else our crazy joint network of people throws our way.

To Jason, I could not have imagined having a better friend and partner through much of this work. You simultaneously brought healthy doses of humour, integrity, and sheer brilliance to all that we did. While I am selfishly sad you have moved on to bigger and better things, I am confident our career paths will cross again.

To Alban, Thanasi, Marc, Mark, and Jonny, thank you for being supportive lab mates

and friends throughout this process. Your work pushes me to be a better and more humble scientist and engineer every day.

To my UROPs these past two years, thank you for bringing energy and ingenuity to all of the many problems you helped me solve. You contributed greatly to this work.

To my students in 2.013 and 2.014, thank you for making my first teaching experiences so enjoyable and enlightening, as well as for inspiring me to be a better and more creative engineer and educator.

For the research itself, much of this work would not have been possible without the financial, technical, and spiritual support of Mike Wardlaw at the Office of Naval Research. I hope we can continue working together in the next phases of this project. Thanks as well to Toray and Swagelok for their generous support of this work.

Contents

List of Figures

List of Tables

Chapter 1

Introduction

As climate change gives rise to more frequent and more devastating severe storms, droughts, and wildfires, an increasing number of communities are facing existential threat due to continual damage to already vulnerable water and electricity infrastructure. For example, according to FEMA, Hurricane Maria in September of 2017 left Puerto Rico without complete power infrastructure well into 2018 after downing 80% of the island's power lines. Additionally, two months after the storm, 30% of the island's inhabitants still lived without direct access to potable water [30]. Clearly, while it is crucial to implement long-term clean energy solutions to curb the onset of climate change, robust short-term solutions for providing portable emergency power and potable water are also necessary. In order to be feasible for the often-remote regions that need them, solutions must be able to utilize resources that are available locally. Additionally, with ground transportation infrastructure easily compromised by natural disasters like hurricanes, floods, and earthquakes, and for countries and territories with limited access to air support, solutions for providing water must be as compact as possible and not require multiple return trips for refueling or equipment maintenance.

One such energy solution that meets these requirements is a water-reactive aluminum-based fuel developed recently at MIT. This fuel is highly energy dense and reacts exothermically with water to produce hydrogen gas and aluminum oxyhydroxide, an inert and valuable byproduct, by the following equation:

$$2\,Al_{(s)} + 4\,H_2O_{(l)} \longrightarrow 3\,H_{2(g)} + 2\,AlOOH_{(aq)} + Q, \tag{1.1}$$

Figure 1-1: Aluminum debris generated in the aftermath of Hurricane Maria in Puerto Rico and Dominica in 2017.

where Q is the heat released by this reaction (11 kWh/L Al). As Fig. 1-1 shows, natural disasters typically generate a significant amount of aluminum debris that usually ends up unused in scrap yards and landfills.

The novel ability to effectively and safely extract energy from scrap aluminum therefore presents inhabitants of drought- and other natural disaster-stricken regions with an environmentally safe and economical solution for dealing with both their water scarcity and aluminum waste issues simultaneously. In particular, coastal countries in Southeast Asia, the Middle East, the Caribbean Islands, and the drought-stricken Western United States stand to benefit greatly from an aluminum debris-powered system, which would enable these regions to convert scrap aluminum to water-reactive fuel, react this fuel with seawater, gray water, or brackish water, generate electricity using the hydrogen reaction product, desalinate or purify water using the reaction's thermal energy output, and provide users with a valuable aluminum oxyhydroxide byproduct that can be sold to offset operating costs. In addition to disaster relief, a compact, robust, and efficient desalination system also has numerous military and civilian applications, ranging from remote base camp resource utilization to emergency desalination on lifeboats. For example, soldiers or first responders could use pre-processed aluminum or utilize aluminum scrap onsite as a high-density energy source for desalinating and purifying their water in the field.

To this end, the focus of this thesis is the design, characterization, and development of a proof-of-concept prototype for a novel method of using the thermal energy released in the aluminum-water reaction to desalinate seawater. First, in order to better understand how much available heat is released by this reaction, a new thermodynamics model is developed and experimentally validated. Subsequently, it is shown that this thermal energy can be used to drive a highly efficient reverse osmosis desalination process without any intermediate energy conversion steps. Finally, the use of this and several key associated technologies also presented here, is explored as a means of significantly improving communities' ability to adapt to climate change by improving their ability to prepare for and respond to natural disasters. The end goal of this work is to shift the way aluminum waste and debris is viewed by giving people the means to turn what would otherwise be considered trash into critical resources like fresh water and electricity in a sustainable way.

1.1 Desalination for Disaster Relief and Preparedness

A "disaster" is broadly defined here as a sudden or unexpected event that causes significant damage and puts human health and safety at risk. Natural disasters like hurricanes and earthquakes, for example, have the capacity to not only threaten human life directly and immediately but can also disrupt critical water and electricity infrastructure, putting millions of people at risk for months afterwards. In the aftermath Hurricane Maria, the number of diabetes related deaths in Puerto Rico increased 46% in the two months after the storm in large part due to power outages preventing insulin from being properly refrigerated. Additionally, the number of sepsis related deaths increased 55% over the same time period as a result of poor sanitary conditions exacerbated by inaccessibility to clean water [26].

At the same time, Puerto Ricans saw an ineffective and slow response from the federal government in providing relief from the effects of this storm. Currently, FEMA's primary solution to providing people with potable water is by transporting water bottles at a net cost of $0.49 per liter after factoring in transportation and logistics costs as well [3]. In the case of Hurricane Maria, FEMA brought bottles to the island but failed to distribute 20 million liters of water, which ultimately were disposed of over a year later in December 2018 [22].

All the while hundreds of thousands of people were without direct access to potable water. Given these current inefficiencies, it is imperative that new technologies be developed and distributed to enable inhabitants of disaster-prone regions to be able harvest local resources to generate their own potable water in preparation for or in response to a natural disaster. Ultimately, technologies have the potential to both save lives and save FEMA significant logistical overhead.

In addition to natural disasters, numerous other events can precipitate an urgent need for potable water. For example, recreational boaters and hikers typically find themselves in remote places without direct access to any water infrastructure that civilization may provide. While preparations can be made to bring the required water along, unforeseen events may cause an unanticipated extension of trip duration or contamination of the water supply. For these cases, a low-cost, highly energy-dense desalination system that could be stored on a lifeboat or in a backpack, for example, would be able to generate the required amount of water for survival until help arrives.

1.1.1 Current Methods for Small-Scale Desalination

The scope of technologies that currently exist for small-scale desalination suitable for disaster relief and preparedness is limited. The scale of interest here ranges from personal to multiple family-sized systems that can desalinate water at rates in the range of 100 to 1000 liters per day. Fig. 1-2 shows some of the state-of-the-art desalinators in this range that are production ready and can be deployed in the event that water is needed in an emergency. As shown here, these devices include solar stills and parabolic reflectors that use solar thermal energy to drive evaporative distillation processes, as well as pumped reverse osmosis systems powered by solar PV or by manual effort.

The single-stage solar still from Aquamate, for example, is extremely simple and cheap, but it is also highly inefficient and therefore would require a significant amount of surface area to scale up produce water at the rate of hundreds of liters per day. At the other end of the scale, multi-stage evaporators that run on solar thermal energy are much more efficient, but due to system complexity and issues with salt scaling, it is impractical to use this technology in smaller, more compact systems. Consequently, there currently does not

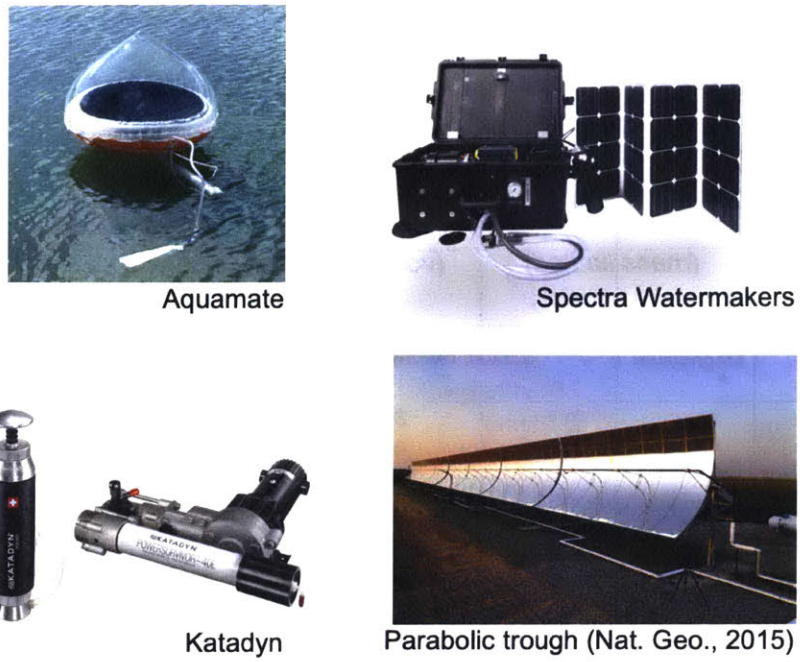

Figure 1-2: Current methods for small-scale desalination (below 1000 L/day) including (clockwise from left) floating solar distillers, fully integrated solar PV powered pumped RO, parabolic trough solar collectors, and manual or ICE-driven pumped RO.

exist an evaporative system that effectively covers the range of output rates targeted here. Additionally, these systems also rely on direct sunlight to provide the energy necessary for desalination, and thus have a potentially low capacity factor, which is not ideal for time-critical disaster relief applications.

Reverse osmosis (RO) desalination systems require pumping saltwater to high pressures against a semipermeable membrane that only allows pure water to permeate through it. These systems can be made compact and minimally complex for the scale of interest here; however, the sources of energy required to power these devices are often suboptimal for this application. In particular, current RO desalinators for disaster relief either require electricity or manual effort to operate the required pumps. In the aftermath of a disaster, grid-supplied electricity is typically unavailable and solar PV runs into similar issues as the evaporative processes with low capacity factors. Human-powered systems, while highly robust, may also be unfeasible if the disaster leaves users partially incapacitated. With human power, there is also a trade-off between the expenditure of often limited metabolic energy and the generation of water that must be considered as well. Accordingly, the design space for providing people

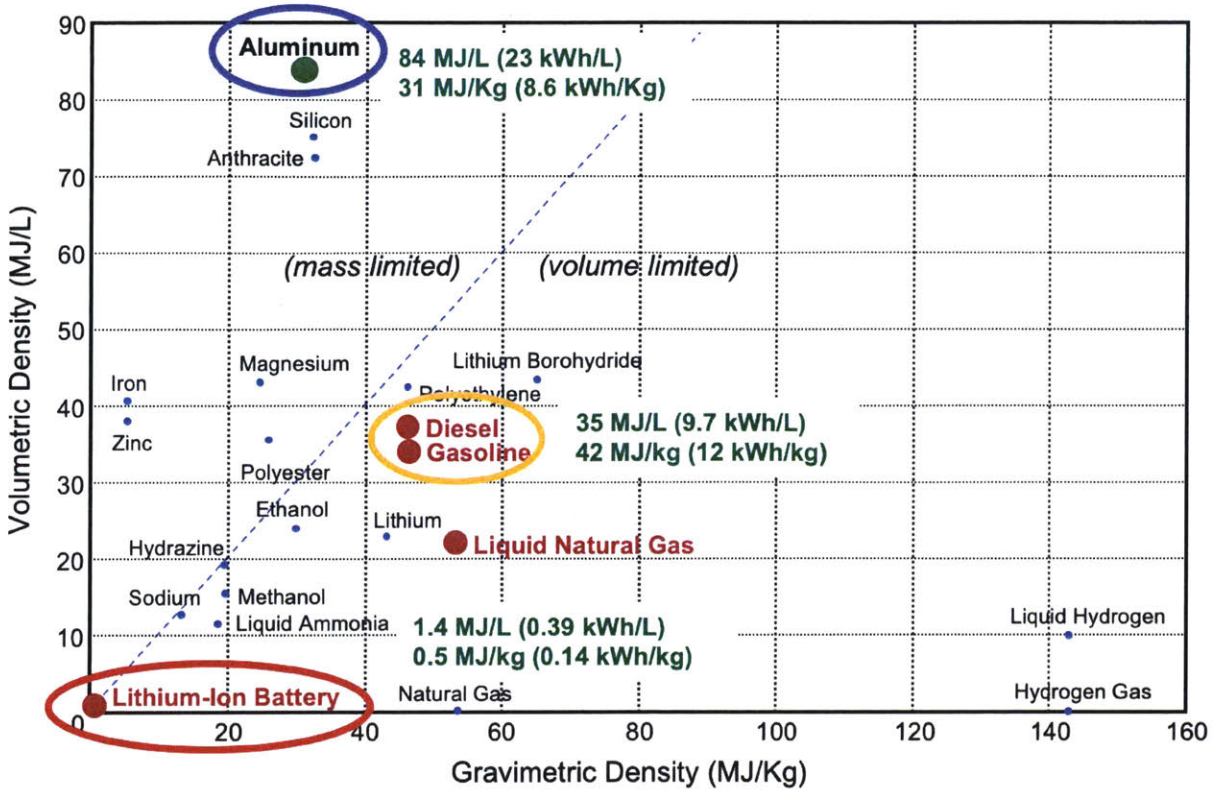

Figure 1-3: Volumetric vs gravimetric energy densities for the most commonly used fuel sources and energy storage technologies.

with an energy-dense, compact, and minimally complex desalinator for use in the aftermath of a natural disaster is still open, a notion that is further supported by the fact that FEMA still ships water bottles as their primary method of providing potable water to people with ready access to contaminated, brackish, or salty water.

1.2 Aluminum Debris as a Fuel Source

As a source of energy for powering desalination, aluminum is highly promising as it is both incredibly energy dense (23.3 kWh/L) and abundant in both the developed and developing world. At two times the energy density of diesel and forty times that of lithium ion batteries, aluminum is one of the most energy dense materials we have ready access to as illustrated by Fig. 1-3. Additionally, only 30% percent of global aluminum production utilizes recycled aluminum, leaving a staggering amount of potential energy sitting idle in landfills across the

Earth, an even more significant issue in developing countries [6]. When natural disasters strike, this collection of unused scrap aluminum grows significantly due to cars and buildings with aluminum structural elements becoming damaged and/or abandoned. Our novel technique converts aluminum from these sources to fuel that, when reacted with water, produces hydrogen and heat, which in turn can be used to generate electricity and desalinate seawater or brackish water directly. The reaction also produces aluminum oxyhydroxide (AlOOH), an inert byproduct which is more valuable than the raw aluminum itself due to its high demand for use in fire suppressants, antacids, antiperspirants, and the manufacturing of pharmaceuticals.

It is important to note here that the production of raw aluminum from bauxite ore is highly energy and carbon intensive. Therefore, even though aluminum is one of the most abundant elements on Earth, its use as a global primary fuel source is neither environmentally safe nor practical. For these reasons, extracting the energy back from aluminum after it has completed its primary function significantly improves the total system efficiency and enables the generation of value for end-users locally. For disaster relief, this means converting aluminum that would end up in a land fill or sold to another country into electricity and potable water locally instead.

1.2.1 Activating Bulk Aluminum

When exposed to air or water, an oxide layer forms immediately on the surface of aluminum, making it functionally inert and unreactive. There have been many techniques for disrupting this oxide layer, including [11], [32], and [27] among others. For this work, aluminum spheres 6 mm in diameter were activated using the technique developed in [28] for its high reaction yields and ease of handling due to its ability to activate bulk aluminum. In this process, aluminum is activated by infusing a gallium-indium eutectic into the grain boundaries via a simple surface treatment [29]. The presence of the liquid eutectic along the grain boundaries allows aluminum ions dissolved within to be transported to water reaction sites at the outer surface. This activation method, which requires only 3% eutectic by mass, allows the treated aluminum to remain mostly inert to oxygen but highly reactive with water. The eutectic is not consumed in this reaction and can be recycled to make new fuel. Additionally, due

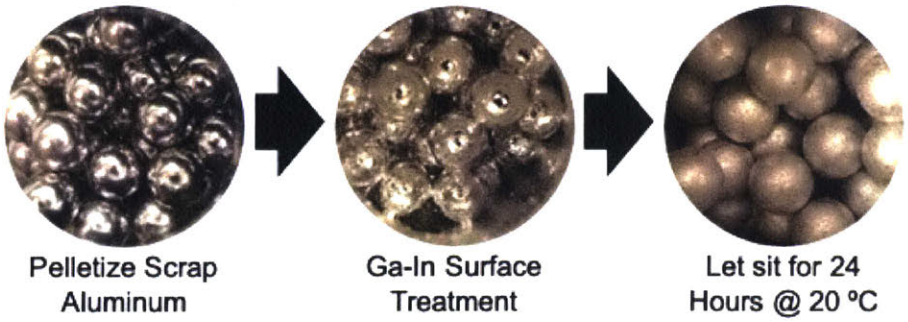

Figure 1-4: Basic process for converting scrap aluminum to a water-reactive fuel using a minimal gallium-indium surface treatment.

to aluminum's high energy density, generating fuel from scrap is a self-sustainable process, requiring 50-100 times less energy than it releases in its reaction with water [13][18].

Fig. 1-4 shows the simple process used to activate aluminum fuel for the purposes of the research presented here. First scrap aluminum is pelletized into uniform, 6 mm diameter spheres and preheated to 120 °C. Next, a eutectic mixture comprised of 80% gallium and 20% indium is heated separately to 120 °C and subsequently added to the aluminum at a mass fraction of roughly 3%. The eutectic-coated spheres remain heated for 90 minutes and are then left to sit at room temperature for 24 hours. Five spheres are typically selected randomly from each batch of activated aluminum, and their reaction yields are tested to ensure that the treatment was done properly. Only batches in which all the tested spheres react to >80% stoichiometric completion are deemed acceptable and used in the experiments presented here.

1.3 Electricity Production from Scrap Aluminum

The reaction between aluminum and water given by Eq. 1.1 releases its internal chemical energy (859 kJ/mol Al) as a mix of thermal energy and chemical potential energy of hydrogen in approximately equal proportions [7]. Fig. 1-5 shows the typical timeline for this reaction, illustrating that within seconds of starting the reaction, a steady flow of hydrogen and steam is produced until all of the aluminum has been converted into the AlOOH byproduct. To generate electricity, the hydrogen produced in this reaction can be used to supply a fuel cell

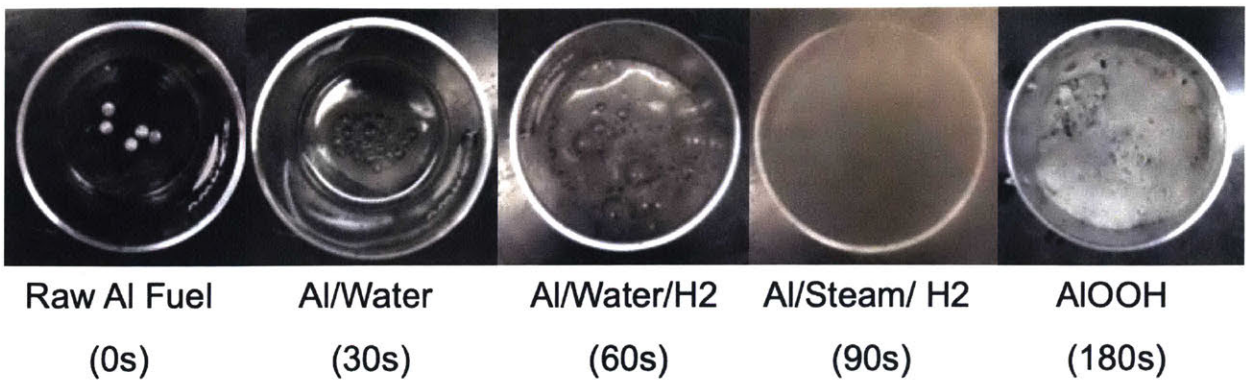

Figure 1-5: Timeline for a typical aluminum-water reaction showing the production of hydrogen, steam, and the final aluminum oxyhydroxide (AlOOH) byproduct.

or internal combustion engine.

Fig. 1-6 shows a novel 3 kW emergency generator built as a final project for 2.013 and 2.014 that consumes aluminum to generate electricity via a fuel cell. In this system, the power generation process begins with the addition of water into a reaction chamber filled with the activated aluminum fuel. This water then initiates an aluminum-water reaction which produces hydrogen gas as well as thermal energy that vaporizes excess water. The output hydrogen from this reaction must then be cooled and purified of steam and other gasses before it can be later consumed by a PEM fuel cell to produce electrical work. This purification is accomplished through a series of heat exchangers and gas purifiers in which the steam is condensed and residual water vapor and oxygen is removed from the hydrogen gas. During this process the steam is recovered and recycled into the system's on-board water tank. Once suitably purified, the hydrogen gas is finally directed into the fuel cell, which converts the chemical energy stored in the hydrogen to electricity at an efficiency of roughly 40%. The output of the fuel cell is pure water, which can be fed back into the reactor to further conserve water consumption in this process.

Fig. 1-6 also shows a system that uses this same process to generate electricity, but on the scale of 20 W. The emergency power pack shown here is comprised of a flexible reaction bladder that contains the pretreated aluminum fuel pellets, a 20 W hydrogen fuel cell, and a standard issue water canteen to supply the water necessary for the hydrogen-producing reaction. In operation, the flexible reaction bladder expands to contain the aluminum oxy-

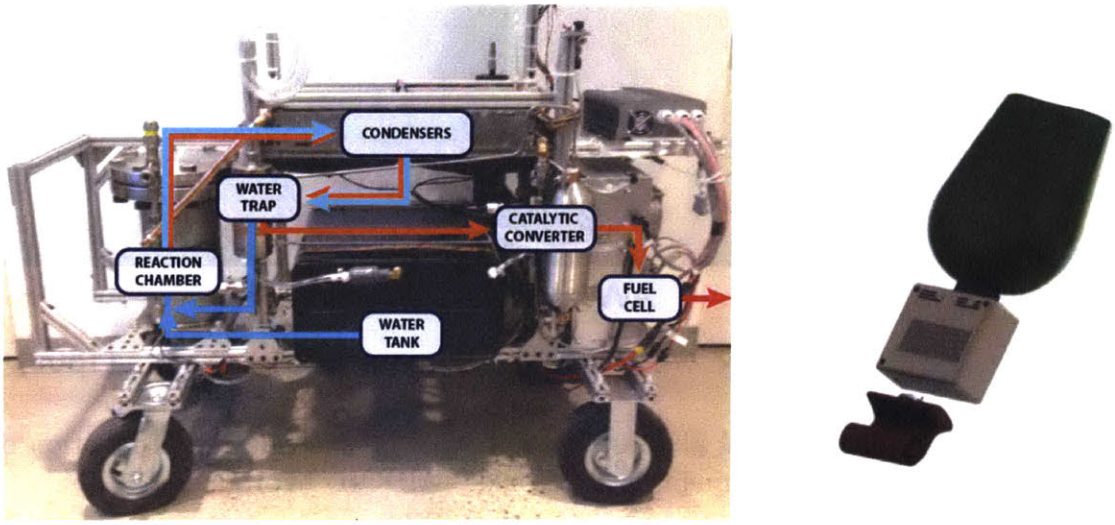

Figure 1-6: Aluminum-fuel power systems for disaster relief applications. Left: 3 kW emergency backup generator. Right: 20 W emergency power pack.

hydroxide waste as hydrogen is produced to supply the small fuel cell. The user can use the electricity generated by the fuel cell to charge a battery, personal communication devices, or other small pieces of equipment in an emergency.

As illustrated by Fig. 1-7, numerous other similar power systems that utilize this aluminum fuel have been developed by the author and others. These power systems all produce electricity via hydrogen fuel cells, allowing them to operate silently and at high efficiency. The reaction of aluminum with water produces no greenhouse gasses or toxic emissions, making these generators usable indoors without concern for noxious emissions as is the case with standard gasoline generators. Additionally, these systems all benefit from the fact that the aluminum fuel developed for these applications has a shelf-life on the order of years. This storage capability is significantly longer than that of gasoline and diesel fuel, a feature which is highly advantageous for such applications as emergency generators or personal energy storage devices where use is infrequent and often unanticipated.

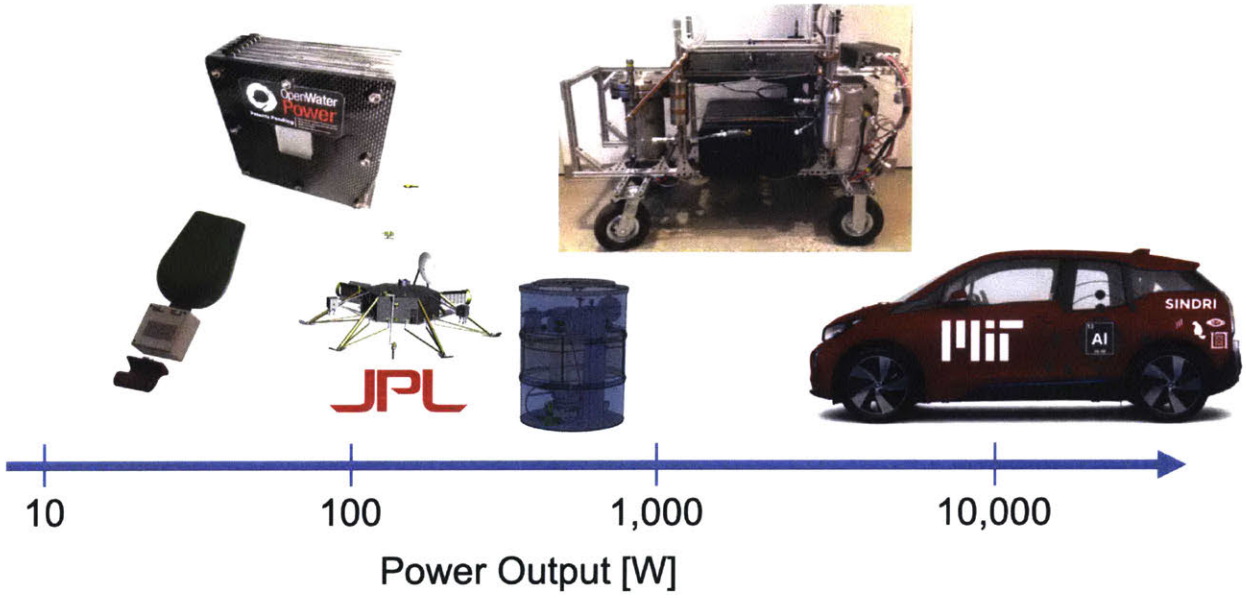

Figure 1-7: Previous applications developed to date that use aluminum as a fuel source for generating electricity. These devices include power systems for a personal emergency power pack, notional JPL Europa lander concept, charging station for drones over the open ocean, and a BMW i3 electric vehicle.

Chapter 2

Aluminum-Water Reaction Thermodynamics

In order to properly design a desalination system that uses the thermal energy released from the reaction of activated aluminum fuel with water, it is first necessary to know how much heat is released in this reaction as a function of system operating temperatures and pressures. In order to model this process, two primary factors must be accounted for. First, aluminum and water can react to form a number of different compounds of the form $Al_xO_yH_z$, and the favorability of each possible byproduct is a function of both temperature and pressure conditions. In addition to affecting the amount of heat released in this exothermic reaction, the formation of different byproducts also informs the amount of water required stoichiometrically for the reaction to proceed, which is a crucial parameter in modeling the performance of any system that uses aluminum as a fuel. Second, because the enthalpies of the species involved in this reaction are themselves functions of temperature, so too is the total enthalpy of reaction (i.e. heat release), which is the net change in enthalpy from the products to the reactants of whichever of the possible reactions is occurring.

Prior work by the US Department of Energy laid the groundwork for this research by compiling results from various sources in the literature in order to map the aluminum-water reaction favorability as a function of temperature [21]; however, their results partially conflict with experimental data given by [31], [5], [11], and [2] and moreover do not include the effects of deviations in pressure. Consequently, the aim of the research presented herein

is the development of a reaction transition diagram which accurately predicts the byproducts of an aluminum-water reaction over a wide range of temperatures and pressures.

2.1 Thermodynamics Model

The temperature and pressure ranges considered for this research were 273.15-600 K and 0.1-10 MPa respectively, and the specific objective of this work was to generate a map of reaction favorability for each of the possible aluminum-water reactions over this parameter space. Because numerous possible reaction byproducts fit the form $Al_xO_yH_z$, it was first necessary to narrow down this list to make the analysis more tractable. In nature, aluminum is found most abundantly in the Earth's crust in bauxite, sedimentary rock comprised of gibbsite ($Al(OH)_3$) and boehmite ($AlOOH$), and in aluminum oxides (Al_2O_3). With this information, coupled with aluminum-water reaction experiments that showed hydrogen being produced in a stoichiometric ratio of 3:2 with aluminum [10], it was hypothesized here that the most likely reactions to occur are:

$$2\,Al_{(s)} + 6\,H_2O_{(l)} \longrightarrow 3\,H_{2(g)} + 2\,Al(OH)_{3(aq)} + Q_1 \tag{2.1}$$

$$2\,Al_{(s)} + 4\,H_2O_{(l)} \longrightarrow 3\,H_{2(g)} + 2\,AlOOH_{(aq)} + Q_2 \tag{2.2}$$

$$2\,Al_{(s)} + 3\,H_2O_{(l)} \longrightarrow 3\,H_{2(g)} + Al_2O_{3(aq)} + Q_3 \tag{2.3}$$

where Q_i indicates the release of heat in each reaction and is itself a function of temperature conditions. This hypothesis was further supported by early work on aluminum-water reactions, which showed conclusively that reactions at 100 °C and 1 bar primarily produce $AlOOH$ [31]. Wider ranges of ambient conditions, however, had not been sufficiently explored previous to this work.

2.1.1 Using Gibbs Free Energy to Predict Reaction Favorability

It is assumed for this analysis that both the temperature and pressure remains constant over the course of the entire reaction. For most power applications running at steady state, this is a reasonable assumption, provided that hydrogen is being produced and consumed at roughly constant and equivalent rates. This key assumption enables the use of the Gibbs free energy to predict reaction favorability over the target operating conditions. Specifically, for each of these candidate reactions, the change in Gibbs free energy, $\Delta G_{rxn}(T,p)$, between the products and reactants is computed in order to determine how thermodynamically favorable that reaction is to proceed. For example, the change in Gibbs free energy for reaction 2.1 would be given by

$$\Delta G^{(1)}_{rxn} = (2 \cdot g_{Al(OH)_3} + 3 \cdot g_{H_2}) - (2 \cdot g_{Al} + 6 \cdot g_{H_2O}), \tag{2.4}$$

where $g_{Al(OH)_3}$, is the Gibbs free energy of $Al(OH)_3$ at a given temperature and pressure.

The sign and magnitude of this quantity indicate whether the reaction in question can occur spontaneously without outside influence and its relative favorability over other possible reactions. Specifically, for $\Delta G_{rxn}(T,p) < 0$, the reaction is spontaneous and for $\Delta G_{rxn}(T,p) > 0$, the reaction will not occur without outside influence. A reaction without a change in Gibbs free energy ($\Delta G_{rxn}(T,p) = 0$) is in equilibrium. When multiple reactions are possible at given ambient conditions, the most favorable reaction is the one that minimizes the change in Gibbs free energy.

Modifying the Gibbs Free Energy for Non-Standard Pressure

Values for the Gibbs free energy for the various species involved in the aluminum-water reaction are given by [17] over a range of temperatures; however, these values are all given at a standard pressure of 1 bar. Consequently, for the analysis presented here, it is necessary to obtain an expression for modifying the standard state Gibbs free energy accordingly. To start, from its definition, the Gibbs free energy G is given by

$$G = H - TS, \tag{2.5}$$

where H is enthalpy, T is temperature, and S is entropy. The differential change in Gibbs free energy, dG, can then be expressed as

$$dG = dH - TdS - SdT, \tag{2.6}$$

where the differential enthalpy, dH, can be similarly derived from its definition as

$$dH = TdS + Vdp, \tag{2.7}$$

where V is the species' volume.

Combining Eq. 2.6 and Eq. 2.7 yields an equation that can be integrated to get the total change in Gibbs free energy over changes in both temperature and pressure:

$$G(T,p) - G^\circ = -\int_{T^\circ}^{T} SdT' + \int_{p^\circ}^{p} Vdp', \tag{2.8}$$

where G° is the Gibbs free energy at standard state temperature, T° (298 K), and pressure, p° (1 bar). Finally, the entropy can be related to the change in Gibbs free energy using the Maxwell relation of

$$S = -\left(\frac{\partial G}{\partial T}\right)_p, \tag{2.9}$$

and can be substituted back into Eq. 2.8 to yield

$$G(T,p) = G(T,p^\circ) + \int_{p^\circ}^{p} Vdp'. \tag{2.10}$$

Here $G(T,p^\circ)$ is given in [17], and thus only the integral over the change in pressure must be computed. For gases, the ideal gas law can be used to express v as a function of temperature and pressure, enabling further simplification of the integral in 2.10 to give

$$G(T,p) = G(T,p^\circ) + nRT\ln\frac{p}{p^\circ}, \tag{2.11}$$

where n is the number of moles of gas present in the system. It is important to note that in Eq. 2.11, p_i is the partial pressure of the gas species, whereas p in Eq. 2.10 is the total ambient

pressure. Once these equations are used to determine the molar change in Gibbs free energy for each compound in a reaction at the desired temperature and pressure, these values can then be subtracted to determine the net change in Gibbs free energy across a total reaction. To do this, the stoichiometric ratios in Eq. 2.1-2.3 are applied to the appropriate expression for molar change in Gibbs free energy and take the difference between the reactants and products, as shown in Eq. 2.4[7].

Additional Model Assumptions

For this analysis, the presence of air or other inert gases is neglected, as well as the formation of steam that could occur due to the exothermic nature of aluminum water reactions. Under certain reaction conditions these effects must be accounted for as well, but because their presence is highly dependent on reaction configurations, it is difficult to generalize their influence. Moreover, the presence of other inert gases is typically negligible as the partial pressure of hydrogen has a minimal impact on the final Gibbs free energy values. The formation of steam, however, could be significant and should be addressed in future work. Finally, it is hypothesized that the precise method of activating aluminum to make it reactive with water would have a negligible effect on the Gibbs free energy, provided that the catalysts strictly do not participate in the reaction. For the particular method of activation previously described, this hypothesis is additionally supported by the fact that the composition of the original elemental aluminum is altered by a mole fraction of only 1%. Even if the gallium and indium used here were to participate in side reactions to some degree, the effects of their presence would be minimal. Finally, for batch desalination using this aluminum-water reaction, the pressures and temperatures may not remain constant over the course of operations. It is recommended that this effect be studied in greater detail in follow-on work.

2.1.2 Model Implementation and Results

To determine which reaction is most favorable at given constant temperature and pressure conditions, we seek the reaction that minimizes $\Delta G_{rxn}(T, p)$. Using values for $g_i^\circ(T)$ given by [17] for $Al_{(s)}$, $H_2O_{(l)}$, $H_{2(g)}$, $Al(OH)_{3(aq)}$, and $Al_2O_{3(aq)}$ and [8] for $AlOOH_{(aq)}$, Gibbs

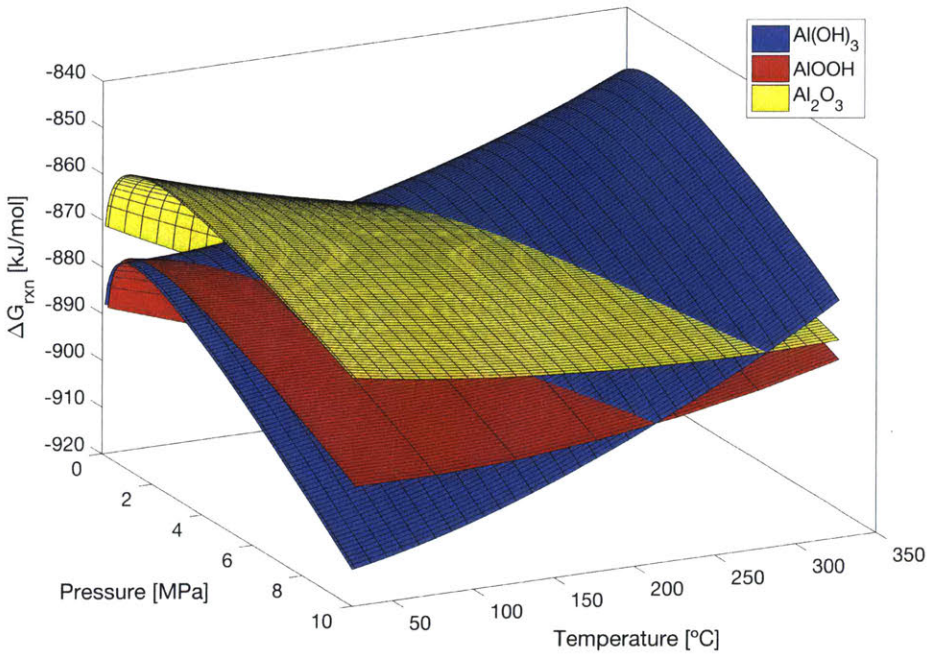

Figure 2-1: Gibbs free energy surface plots for each candidate aluminum-water reaction over operating range.

free energy values for each of the three candidate aluminum water reactions were computed. These values were then evaluated in MATLAB over grid of 3700 points in a range of 273.15-600K and 0.1-10 MPa. Because the temperature data was comparatively sparse, this program iterates over pressures, at every step computing the Gibbs free energy for each available temperature data point and interpolating using a second order polynomial. Sweeping these curve-fit polynomials over the target operating pressure range generates the surfaces shown in Fig. 2-1. Additionally, to highlight the transitions between each reaction regime, this code also computes

$$\min_i(\Delta G^{(i)}_{rxn}(T,p)) \tag{2.12}$$

in order to show the regimes in which each reaction, i is most favorable. Fig. 2-2 shows the curves that represent the transitions between these regimes and can be used generally to determine the expected reaction for given operating conditions. At atmospheric pressure for example, the reaction producing $AlOOH$ is more favorable above 21 °C and the reaction

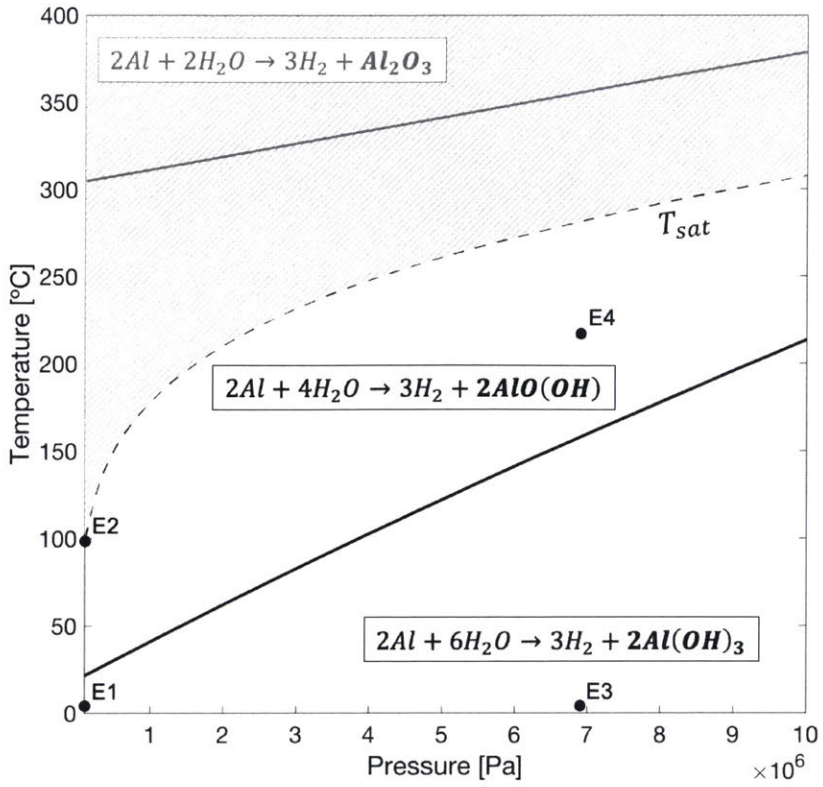

Figure 2-2: Aluminum-water transition diagram showing the different temperature-pressure regimes in which the labeled reactions are most likely to occur. Above the water saturation curve, T_{sat}, reactivity may be severely inhibited depending on the method of aluminum activation. Labels E1-E4 correspond with the conditions used for experimental validation.

producing $Al(OH)_3$ is more favorable below 21 °C.

Modifying Model for Limited Steam Reactivity

With the particular method of aluminum activation employed for this research first developed in [28], it was found that these activated aluminum pellets exhibit no observable reaction with steam. Consequently, the reaction regime transition diagram is modified accordingly to show limited reactivity above the saturation temperature, $T_{sat}(p)$, for water at a given pressure, since above $T_{sat}(p)$, liquid water will rapidly vaporize at the surface of the aluminum in practice, severely inhibiting the reaction. The shaded area of the diagram in Fig. 2-2 shows this region of limited reactivity. The thermodynamics analysis presented here does not take this phenomenon into account, however, and thus for different methods of aluminum activation, this inhibited ability to react with steam may not be present. In this case, the

Figure 2-3: High temperature and pressure test apparatus used for validating the thermodynamics model presented here [25].

shaded region here can be ignored.

2.2 Experimental Validation

To validate the thermodynamics model for predicting which aluminum-water reaction is most favorable at given temperature and pressure conditions as shown in Fig. 2-2, four reaction experiments were performed toward the extremes of the target operating range as indicated on the same figure by the points labeled E1-E4. Two high-pressure tests (E2 and E4) saw the reaction of aluminum and water in a pressure vessel maintained at 6.9 MPa and at temperatures of 230 °C and 4 °C. Two atmospheric pressure tests (E1 and E2) saw the reaction of water and aluminum at 100 °C and at 4 °C. These operating points were chosen so as to provide two data points above and below the curve that represents a transition between the $Al(OH)_3$ and $AlOOH$ reaction regimes.

For the high pressure experiments, the test apparatus shown in Fig. 2-3 was used to

maintain a constant 6.9 MPa over the course of the reaction. This setup is comprised of stainless steel tubing and Swagelok fittings to ensure minimal leaking. Nitrogen gas was used to pre-pressurize the reactor and the system pressure was maintained via a pressure relief valve. Note that the presence of nitrogen in this analysis is neglected as it only affects the hydrogen term in $\Delta G_{rxn}(T, p)$. Due to the stoichiometry, this deviation reduces $\Delta G_{rxn}(T, p)$ for each candidate reaction by the same amount, and thus there is no effect on where the transitions between each reaction occur.

Activated aluminum samples are initially held in a tube above the reactor by means of a servo-driven ball valve, which enabled us to remotely deliver the samples to the water in the reaction tube below. Due to safety considerations, the entire experiment was performed remotely. For the high temperature and high pressure experiment, the reactor and sample pre-feeder tubes were preheated to the specified temperature of 230 °C using a manually-adjusted resistive heating strip wrapped around the tubes. Fiberglass insulation, not pictured in Fig. 2-3, was added around the heating elements.

In the high pressure and low temperature experiments, the entire test apparatus was placed in a large cooling chamber maintained at 4 °C for the duration of the experiment. The apparatus, water, and aluminum were pressurized and pre-chilled for one hour, and again the aluminum samples were delivered to the reactor below via remote activation. Given the greatly reduced reaction rate of aluminum and water that has been observed at low temperatures, the apparatus was left undisturbed for 48 hours to ensure the reaction would proceed to completion.

For the 100 °C, atmospheric pressure experiment, water in an open beaker over a hot plate was brought to a boil, and aluminum samples preheated to 100 °C were subsequently added. To keep the system cool for the experiment at atmospheric pressure and 4 °C, a small amount of aluminum was reacted in a large, constantly stirred, ice bath. A temperature probe placed near the reaction site confirmed that the reaction was kept below 4 °C.

In all cases, the aluminum-water reaction byproducts, which were crucial for determining which reaction occurred, were dried at room temperature in a clean and uncontaminated fume hood for one week before their composition was analyzed. This drying step was crucial, as some analysis techniques like FTIR are highly sensitive to the presence of water.

Trial	T [°C]	p [MPa]	$\Delta G_{rxn}^{(i)}$ [kJ/mol]	Expected Byproduct	Actual Byproduct(s)
E1:	4	0.1	-887	$Al(OH)_3$	Elemental Al, $Al(OH)_3$
E2:	100	0.1	-897	$AlOOH$	$AlOOH$
E3:	4	6.9	-898	$Al(OH)_3$	$Al(OH)_3$
E4:	230	6.9	-880	$AlOOH$	$AlOOH$
Steam:	150	0.1	N/A	Al_2O_3	No reaction

Table 2.1: Summary of results for reaction experiments spanning target operating range.

In addition to residual water resulting in inaccuracies in the FTIR measurements, there are two other potential sources of error to acknowledge. First, because the aluminum-water reaction is exothermic, localized heating of the activated aluminum pellet could result in actual temperature conditions that are higher than intended. This was mitigated by maintaining the temperature of the surrounding reaction site at a constant temperature and by only reacting small amounts of aluminum at a time. Additionally, impurities in the water could result in side reactions, the products of which may be detected by either the FTIR or XRD equipment. With this in mind, deionized water was used in all experiments as a precaution.

2.2.1 Byproduct Composition Analysis

Two sets of experiments were performed to determine the composition of the aluminum-water reaction byproducts. First, an FTIR method was used to obtain IR spectra for the byproduct samples. Here a standard technique was used in which potassium-bromide (KBr) is mixed with some reaction byproduct sample and compressed to produce a pellet. The IR spectrum for each pellet was measured using a Thermo Fisher FTIR6700 spectrometer in transmission mode over a range of 400-4000 cm^{-1} and with a resolution of 1.93 cm^{-1}. Second, XRD was performed using a Shimadzu XRD-6000 Lab-X diffractometer with a copper source ($\lambda = 0.15406$ nm) over a range of 10-90°at a resolution of $0.02°(2\theta)$.

The results of the reaction transition diagram presented here were validated using FTIR and XRD, as summarized in Table 2.1. For experiment E1, XRD results were inconclusive as the limited reactivity at lower temperature and atmospheric pressure left enough elemen-

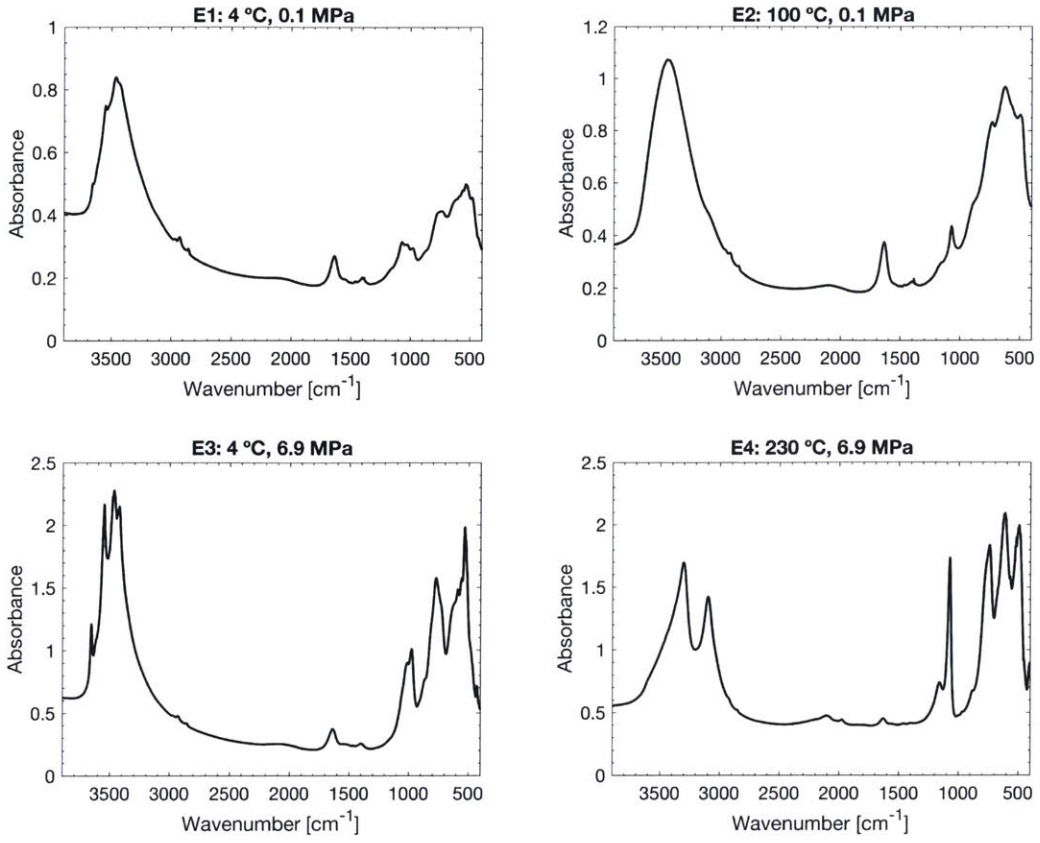

Figure 2-4: FTIR results for the reaction byproducts collected for experiments E1-E4.

tal aluminum in the byproducts to saturate the readings and prevent the detection of any hydroxide. The IR spectrum for this sample, as shown in Fig. 2-4, however, exhibits peaks in the locations of the characteristic hydroxyl stretching and bending modes for gibbsite ($Al(OH)_3$) [14]. In particular, distinct peaks are shown in the 3656, 3548, and 3464 cm^{-1} bands, with a slight shoulder at 3430 cm^{-1}, all of which are indicative of $Al(OH)_3$. Characteristic Al-O stretching, as identified in [24], is indicated by peaks in the 482.1, 532.3, and 721.3 cm^{-1} bands and further supports the formation of $Al(OH)_3$.

For experiment E2, both XRD and FTIR results indicate a strong presence of pseudoboehmite. XRD results, shown in Fig. 2-5, indicate a close match with the ICDD reference for $AlOOH$ [12], and FTIR results strongly indicate the characteristic hydroxyl stretching mode at 3442 cm^{-1} with a weak shoulder at 3101 cm^{-1}. The absence of strong peak definition in higher wavenumbers for this sample indicates the presence of additional water in

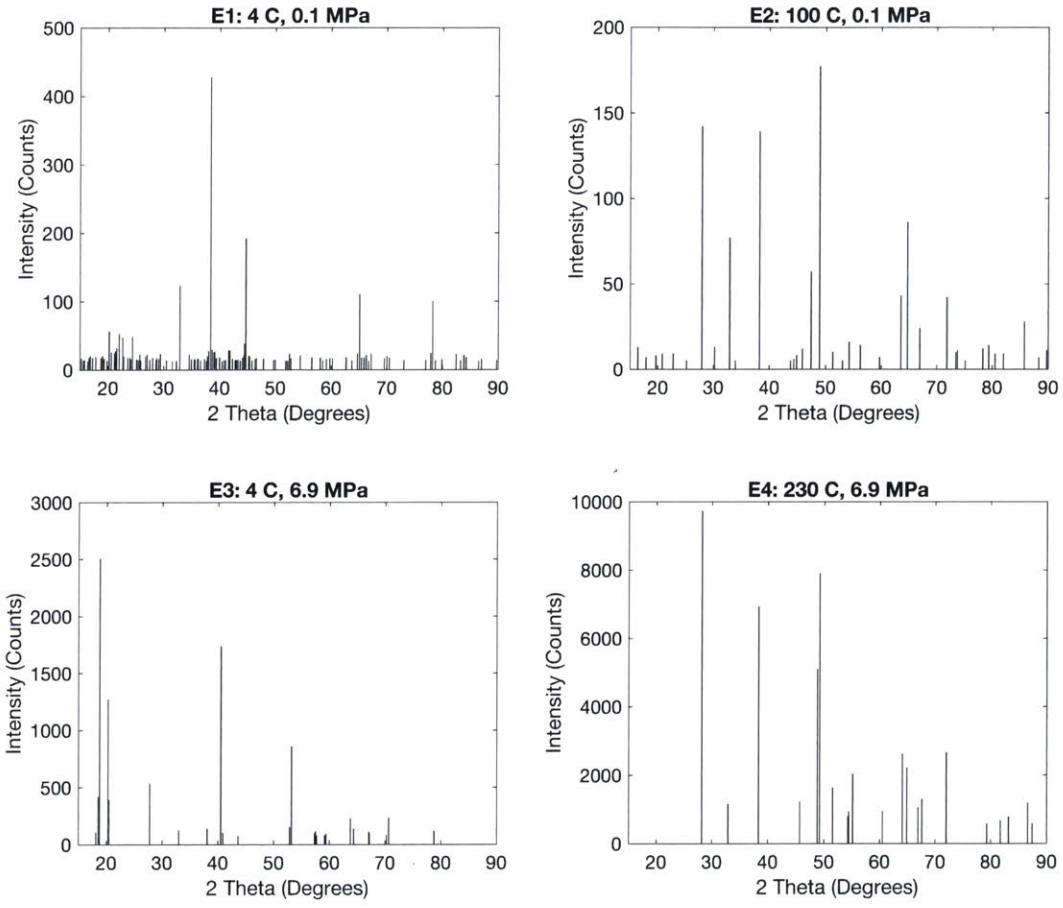

Figure 2-5: XRD results for the reaction byproducts collected for experiments E1-E4.

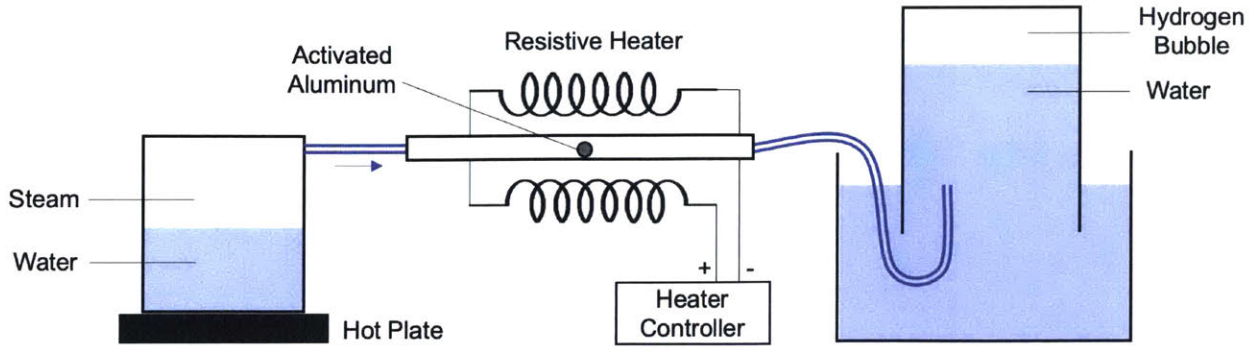

Figure 2-6: Experimental setup for testing the reactivity of aluminum with steam.

the sample and thus suggests that its composition is primarily pseudoboehmite. This result is corroborated via comparison with the spectra for pseudoboehmite obtained in [31]. As before, the same characteristic Al-O stretching modes are exhibited by peaks in the 495.6, 626.8, and 732.8 cm^{-1} bands.

Experiments E3 and E4 showed strong matches to reference data for $Al(OH)_3$ and $AlOOH$ respectively in both the XRD and FTIR analyses. In particular, for E3, strong and well-defined peaks in the IR spectrum at the 3656, 3548, 3465, 3435, 3423, 977.7, 771.4, 530.3, and 430.0 cm^{-1} bands support the independent XRD match to ICDD reference data for $Al(OH)_3$. For E4, peaks in the IR spectrum at the 3307, 3095, 1074, 742.5, 613.3, and 493.7 cm^{-1} bands are in close alignment with data given by [31] and [14] and corroborate this collected XRD data, which indicated a match to $AlOOH$. The 742.5, 613.3, and 493.7 cm^{-1} bands in particular indicate the expected Al-O stretching. The model presented here is additionally supported by prior work in [31], [5], [11], and [2], in which aluminum-water reactions were shown to primarily produce $AlOOH$ at 1 bar and temperatures above 50 °C.

2.2.2 Testing the Reactivity of Aluminum With Steam

To determine the reactivity of aluminum with steam, the setup shown in Fig. 2-6 was used. In this setup, steam is produced by boiling water over a hot plate and is subsequently passed through a pre-heated glass tube containing the aluminum sample. The tube heater here is a simple resistive heater controlled manually using a thermocouple for feedback. Steam and resultant hydrogen leave this heated tube and bubble up through a water column con-

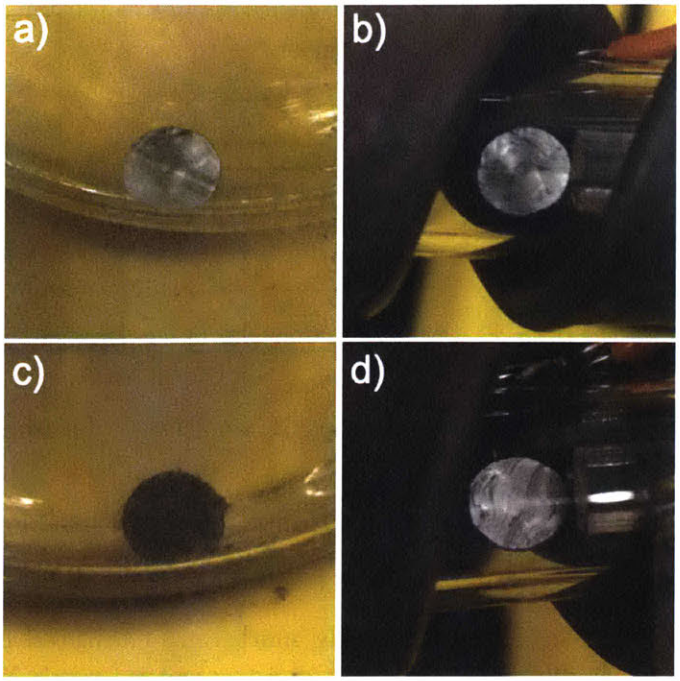

Figure 2-7: Results from steam reactivity tests. a) and c) depict the same activated aluminum sample exposed to 100% RH air at room temperature 35 minutes apart, and b) and d) depict an activated aluminum sample exposed to superheated steam 35 minutes apart. The darkened grey surface of the sample in c) indicates the presence of $AlOOH$.

tained in an inverted beaker, allowing us to measure the volume of any hydrogen produced. Throughout this process, the temperature of the aluminum sample, and walls of the tube holding it, are kept well above $T_{sat} = 100$ °C at atmospheric pressure to ensure steam does not condense on the sample, potentially skewing the results. Additionally, it was useful to use a transparent tube in order to visually inspect the degree of reaction, which is typically marked by a distinct discoloration of the aluminum. Finally, as a control the same amount of activated aluminum was placed in a jar of argon maintained at 100% relative humidity and at a room temperature of 20 °C. This added step was for visual comparison to assess the relative degree of reaction between the two samples.

In the experiment for determining the reactivity of steam with the activated aluminum, no hydrogen was measured in the bubble column setup shown in Fig. 2-6. Additionally, visual inspection of the aluminum sample at various points during the experiment also failed to detect the presence of any hydroxide accumulation on the surface, which can be marked by a distinct darkening discoloration and would indicate the presence of some reaction. Fig.

T [°C]	$\Delta h_{rxn}^{(1)}$ [kJ/mol]	$\Delta h_{rxn}^{(2)}$ [kJ/mol]	$\Delta h_{rxn}^{(3)}$ [kJ/mol]
0	-866.0	-845.4	-815.4
25	-872.0	-849.4	-818.2
50	-877.6	-853.1	-820.8
75	-882.9	-856.8	-823.4
100	-887.9	-860.3	-825.9
125	-892.8	-863.8	-828.3
150	-897.6	-867.2	-830.8
175	-902.4	-870.8	-833.3
200	-907.1	-874.2	-835.8
225	-911.9	-878.0	-838.5
250	-917.0	-881.9	-841.4
275	-922.6	-886.3	-844.6
300	-929.1	-891.3	-848.4

Table 2.2: $\Delta h_{rxn}(T)$ [kJ/mol] per two moles of aluminum for the three aluminum-water reactions shown in Eq. 2.1-2.3.

2-7 shows the surface of the activated aluminum sample within the test apparatus during operation at the beginning of the experiment in b) and 35 minutes later in d). In the control sample, which was maintained in argon gas at 100 % relative humidity and 20 °C, a discoloration is apparent between a) and c) in Fig. 2-7, again taken at the beginning of the experiment and 35 minutes later respectively, indicating that some reaction was occurring on the surface. The use of argon, which is more dense than air at 20 °C, rules out oxidation as a cause for the discoloration, suggesting that differences in the adsorptivity of water to the surface of the aluminum at varied temperatures is the likely cause of these results.

2.3 Thermal Energy Release

The results of this work are an accurate model for the conditions under which each possible aluminum-water reaction is most favorable to occur. This model enables the prediction of how much water is required stoichiometrically for the reaction to proceed, as well as how much heat is released. Within each reaction regime, this heat release is also a function of temperature, as the enthalpy for a given species is given as

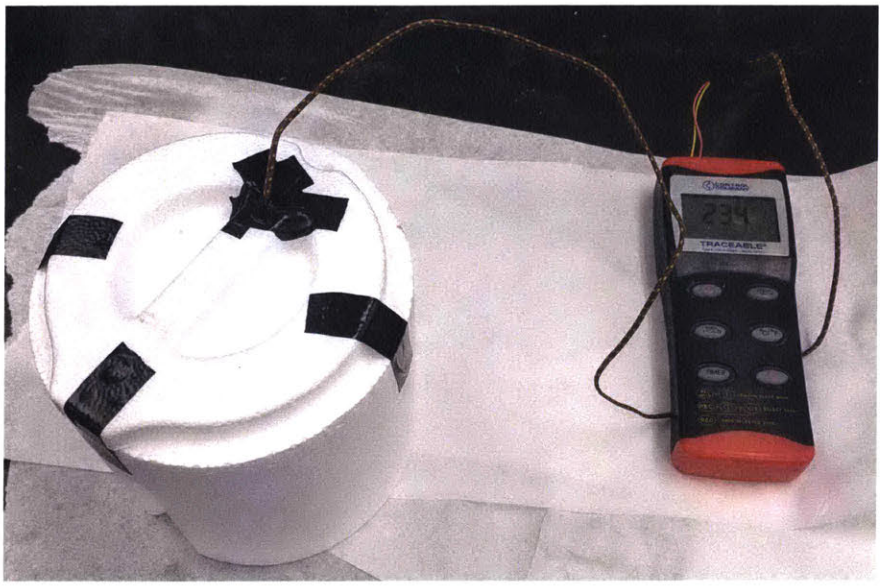

Figure 2-8: Calorimetry setup for measuring the aluminum-water reaction heat release.

$$h_i(T) = h_i(T_0) + \int_{T_0}^{T} c_p dT', \tag{2.13}$$

where T_0 is some arbitrary reference temperature for which $h_i(T_0)$ is known and c_p is the specific heat of the species. The enthalpy of reaction, $\Delta h_{rxn}^{(i)}$, is then given as the net difference in the enthalpies between the product and reactant species. The results of this analysis are tabulated here in Table 2.2.2 for a selection of temperatures and can be used to design applications which utilize this heat release.

Preliminary calorimetry results using a test setup shown in Fig. 2-8 show initial alignment with these values presented here for the *AlOOH* reaction held at 25 °C. This test apparatus consists of a simple insulated water bath of known volume, into which the activated aluminum samples are placed. The temperature rise of the water is measured, and the heat release is subsequently computed. This test setup was calibrated using a resistive heater dissipating a known quantity of energy into the water bath. It is recommended that in future work, a more comprehensive calorimetry experiment be conducted to measure this heat release over a wide range of temperatures and pressures in order to further validate these results.

Chapter 3

Heat-Driven Reverse Osmosis (HDRO)

A primary goal of this research was to develop a system for using activated aluminum fuel to power the production of potable water for disaster relief or preparedness at comparable efficiencies to existing solutions and at reduced cost and resource consumption. The products of an exothermic aluminum-water reaction can be used to desalinate seawater or purify contaminated water in a plethora of ways. For example, the hydrogen product of this reaction can be used to generate electricity efficiently using a fuel cell or internal combustion engine-type generator, which can in turn can power a pumped reverse osmosis (RO) system or vacuum-driven multi-effect distillation (MED) system. In the context of small scale disaster relief or larger scale climate change resiliency, however, it may be advantageous instead to use this electricity to power other critical processes and devices like lighting, communications, or medical equipment. Consequently, with these applications in mind and given the fact that a significant amount of thermal energy is released in the aluminum-water reaction (11 kWh/L or 4 kWh/kg Al), only heat-driven desalination processes were considered in this research.

To narrow the scope of candidate technologies further, the scale targeted for this research prohibits the effective use of MED and multi-stage flash distillation (MSF), both of which require numerous large flash chambers that result in high efficiencies but do not scale down well. Without the benefit of additional flash chambers that allow for repeated recycling of the evaporated water's latent heat, single stage evaporative desalination processes, while compact and minimally complex, have low efficiencies compared to RO. For these applications, RO was identified as an ideal technology in terms of simplicity and energy efficiency; however,

existing solutions for powering RO at the target scale require electrically or manually driven pumps. In the aftermath of a natural disaster, electricity is often unavailable and manual effort may be difficult if users are partially incapacitated or must conserve metabolic energy due to limited food supply. Thus, an RO system which can run off thermal energy with no intermediary energy conversion was targeted as an ideal candidate solution, and the design and characterization of a novel system that accomplishes this goal is presented here.

3.1 Overview and Operation

There are numerous applications that necessitate providing fresh water using a system that is physically compact and highly energy dense. For disaster preparedness, for example, users may need to store this system for months to years before it is used, and thus a system that can remain ready to use and out of the way is desired, especially for use in space-constrained homes and boats. Additionally, because of the possibility of needing to store this device for a significant length of time, the system also has to be minimally complex with parts that do not degrade over time. With this in mind, the following design constraints were set for the development of this desalination device:

1. No or as few moving parts as possible to minimize points of failure
2. No electricity or manual effort required
3. Scaled for single or multi-family usage
4. Volumetrically compact and energy efficient
5. Economical (comparable to FEMA's water cost of \$0.49/L [3])

To this end, the system shown in Fig. 3-1 was developed to provide a compact and minimally complex system for purifying water at high efficiencies. This system employs a novel method of desalination that is first named here as "Heat Driven Reverse Osmosis", hereafter referred to as HDRO, in which the thermal energy from an aluminum-water reaction (or any exothermic chemical reaction, external heat source, etc.) is used to drive reverse

osmosis directly without any intermediary heat engines or thermoelectric generators. In fact, as is explained in detail below, this process effectively turns the desalinator itself into a heat engine directly.

3.1.1 Reverse Osmosis

In its basic operation, HDRO involves the release of heat in an enclosed vessel to generate the high pressures required for driving reverse osmosis, a membrane-based separation process in which water with salts or other contaminants is pressurized against a selectively permeable membrane that only allows water to permeate through it. These membranes are typically made from polyamide and additionally prevent other common solutes, molecules, bacteria, etc. from passing through, leaving highly pure water on the permeate side. Fig. 3-3 shows a simple graphical depiction of the basic operating principle behind reverse osmosis.

Reverse osmosis, as the name implies, is not a thermodynamically favorable process; in order to drive this process, high pressures on the order of 34-50 bar for typical seawater are required to overcome the natural affinity for water to dissolve back into the feed solution. The lower the concentration of water in the feed solution, the higher is this "osmotic pressure" required to separate it out from the solution. Typically, this pressure is provided using electrically or manually driven pumps. The minimum work required by these pumps to separate pure water from a salt solution is given by the change in exergy, Ξ, between the inputs and outputs of this system as

$$W_{min} = \Xi_{min} = \sum_{out} n_p g_i(T,p) - \sum_{out} n_p g_i(T,p), \tag{3.1}$$

where n_p is the number of moles of water desalinated and g_i is the molar Gibbs free energy of a particular species i at temperature T and pressure p.

In a batch RO process, if $RR * n_f$ moles out of n_f initially are desalinated, where RR is some recovery ratio between 0 and 1, this minimum work can be expressed as

$$W_{min} = n_p * \left[(g_p - g_c) - \frac{1}{RR}(g_f - g_c) \right], \tag{3.2}$$

where the subscripts p, c, and f refer to permeate (desalinated water output), concentrate

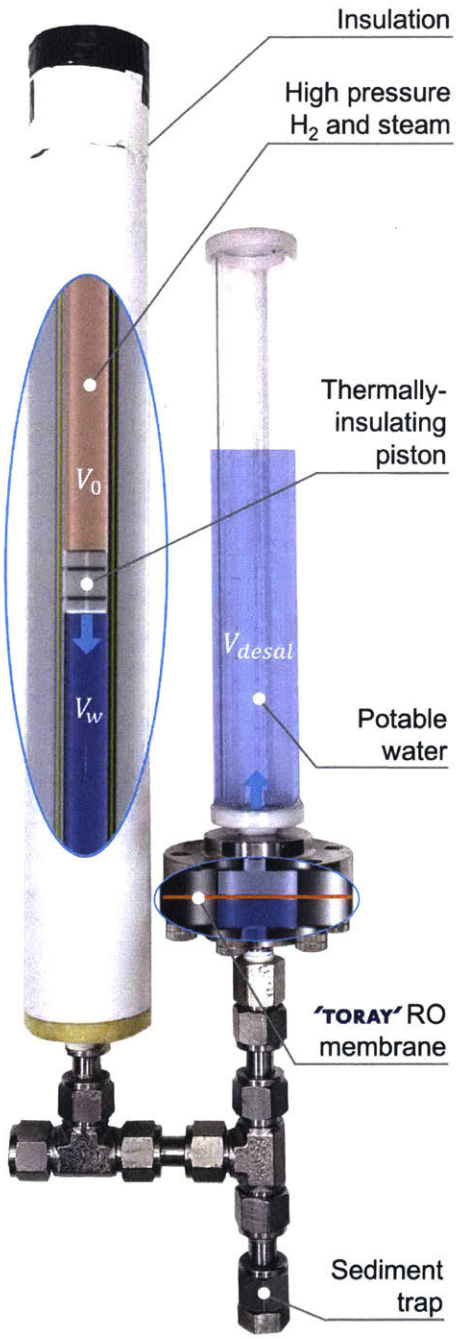

Figure 3-1: HDRO prototype system using an exothermic aluminum-water reaction to drive seawater desalination.

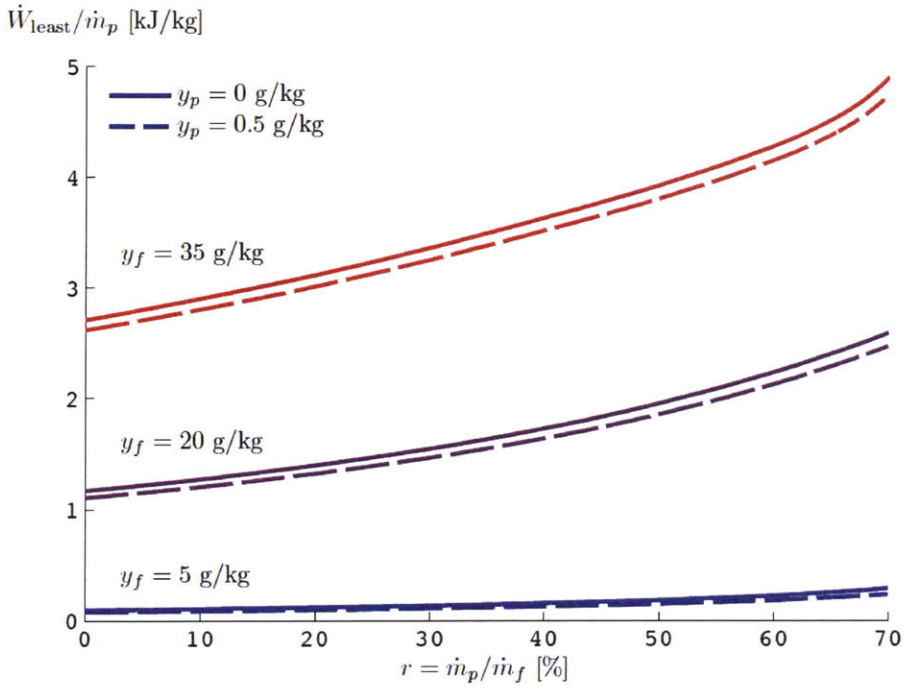

Figure 3-2: Minimum work per unit output required to desalinate saltwater at various salinities [19].

(saltwater left behind), and feed (initial saltwater input) respectively. This quantity was plotted for various input and output salinities by [19] and is reproduced here in Fig. 3-2. As a point of reference, pumped RO operating on 3.5% salinity saltwater at a recovery ratio of 0.5 requires a minimum of roughly 1 Wh per liter desalinated.

3.1.2 Underlying HDRO Principles

In typical RO systems, however, the actual work required increases significantly due to pump inefficiencies, frictional losses, and concentration polarization effects at the membrane [23]. The novelty of HDRO is that no pumps are required and therefore pumping losses can largely by avoided. Instead the pressure is generated by some thermal energy release directly. By the ideal gas law, we have the simple relationship between pressure, temperature, and density of the gas in the system given as

$$P = \rho RT, \tag{3.3}$$

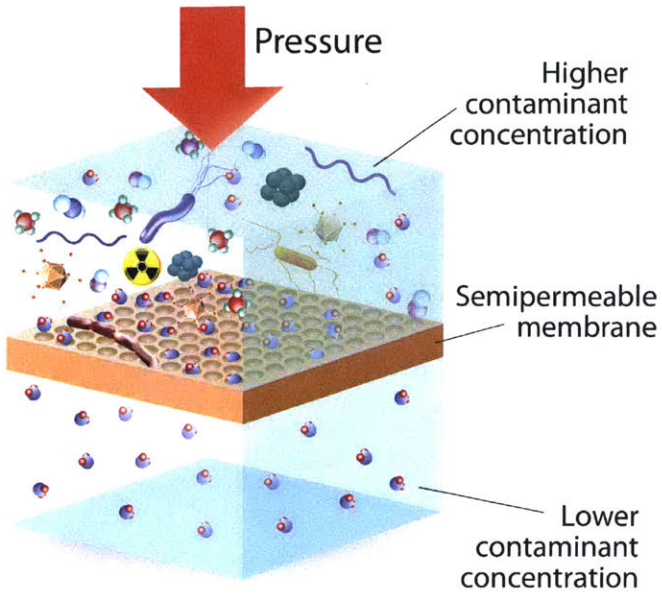

Figure 3-3: Graphical depiction of a reverse osmosis water separation process using a membrane that is selectively permeable to water [Advanced Water Solutions, 2018].

so simply put, if the temperature or the density of the gas increases, so too does the pressure. In the case of an aluminum-water reaction driving this process, there are three factors that contribute to increasing the pressure: 1) the thermal energy released due to the exothermic nature of this reaction goes into raising the temperature the gases in the enclosed vessel, 2) water and aluminum react to form hydrogen gas, increasing the density of the gas in the vessel as its volume remains constant, 3) increased temperature inside the reactor increases the vapor pressure of any additional two-phase solutions present (e.g. excess water).

In the HDRO process, an enclosed vessel with a semipermeable membrane on one end is partially filled with seawater or water with other contaminants. The aluminum-water reaction or equivalent is then used to increase the pressure of the vessel as previously described, subsequently forcing pure water through the membrane. This type of "dead-ended" configuration desalinates water in batches, leaving the salt and other contaminants to remain in the feed solution over the course of the HDRO process. As such, the osmotic pressure continually increases as the concentration of water in the feed solution continually decreases. Additionally, as more and more water is removed from the solution, the volume of the gas is allowed to increase, thereby lowering its pressure by the ideal gas relation. Consequently,

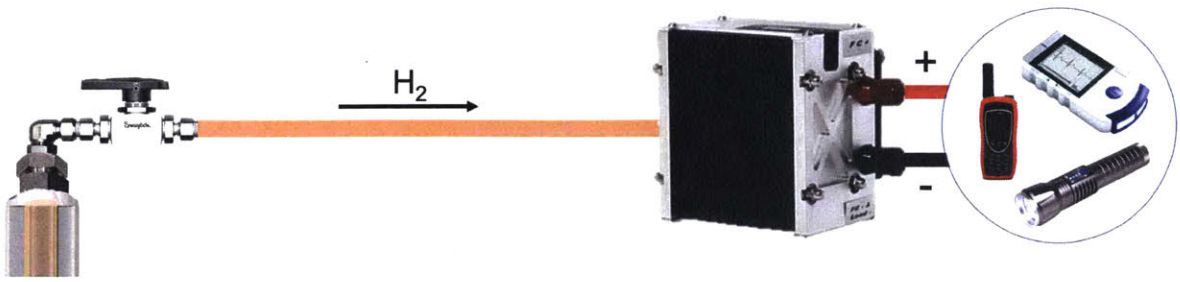

Figure 3-4: After HDRO using an aluminum-water reaction is complete, the generated hydrogen gas can be used to supply a fuel cell to produce electricity, for example.

the system must start with a sufficiently high pressure to remain above the time-varying osmotic pressure over the course of this reaction. For the system described in detail in the following section, this pressure is the maximum pressure that the materials used to manufacture the reaction vessel can withstand. For 1-inch diameter stainless steel tubing with a wall thickness of 0.12 inches, this pressure with a reasonable safety factor is 138 bar.

It is important to note that because the total work done by this system is the integral of pressure times volume, this over-pressure results in a sub-optimal desalination process from a second law efficiency perspective; however, it is shown in the following section that HDRO is still up to 41 times more efficient than simply boiling the saltwater. Further, it is possible to reduce this over-pressure using techniques discussed in greater detail later in this thesis.

3.1.3 HDRO Operation

To operate the system shown in Fig. 3-1, activated aluminum fuel pellets and water, for example, are placed in the top half of the pressure vessel in the volume labelled V_0. The pressure builds to 138 bar, and pure water is forced through the reverse osmosis membrane until the pressure in the reactor drops to the osmotic pressure. A thermally insulating piston separates the reaction from the feed solution both as a means of insulating the hot gasses to improve efficiency and to prevent additional contaminants from entering the feed solution. In principle, this piston is not required, but it serves to significantly improve system performance.

After desalination, because the hydrogen generated by the aluminum-water reaction was only acting as the working fluid driving this process, it can be used after desalination is

complete to either produce electricity using a fuel cell or internal combustion engine-type generator or can be burned to provide additional heat for cooking or additional water decontamination. For example, Fig. 3-4 shows how this hydrogen can be diverted to a fuel cell using a simple valve at the top of the HDRO device. This functionality also emphasizes that only the thermal energy released in the aluminum-water reaction (11 kWh/L Al) is consumed by the desalination process, leaving the remaining energy stored as the hydrogen's chemical energy (12 kWh/L Al) to be utilized in some other way later.

With a basic understanding of HDRO established, it is necessary to analyze this process in further detail to understand exactly how much aluminum and water is required to drive this process, as well as how the system scales with the percentage of water extracted from the initial feed solution. The following sections detail the thermodynamics behind this process with the ultimate goal of providing a set of design tools for sizing this type of system based on user constraints of volume or energy efficiency. Further, the results of an initial prototype are presented here, as well as suggestions for improving the system modeling and efficiency.

3.2 Thermodynamics Model

The dead-ended batch HDRO process developed here can be modelled as three separate states, which are depicted graphically by Fig. 3-5. In State 1, at time $t = 0$, activated aluminum fuel pellets and liquid water are placed in the top portion of a enclosed piston, which is enclosed on one end by a semipermeable RO membrane. Below the piston sits seawater with some initial known salt concentration, C_0. The height of the piston is set such that the volume of the top portion containing the fuel reactants is initially at V_0, the volume of the bottom portion containing the seawater is V_w, and the total volume, V_T, is equal to $V_w + V_0$. The entire piston is initially at atmospheric pressure and temperature, P_{atm} and T_0 respectively.

It is assumed here that the rate of reaction is much greater than the rate of desalination in this configuration and consequently that all of the aluminum fuel and water react to produce hydrogen and aluminum oxyhydroxide before any significant amount of water is desalinated. This assumption is empirically consistent with both reaction and desalination permeation

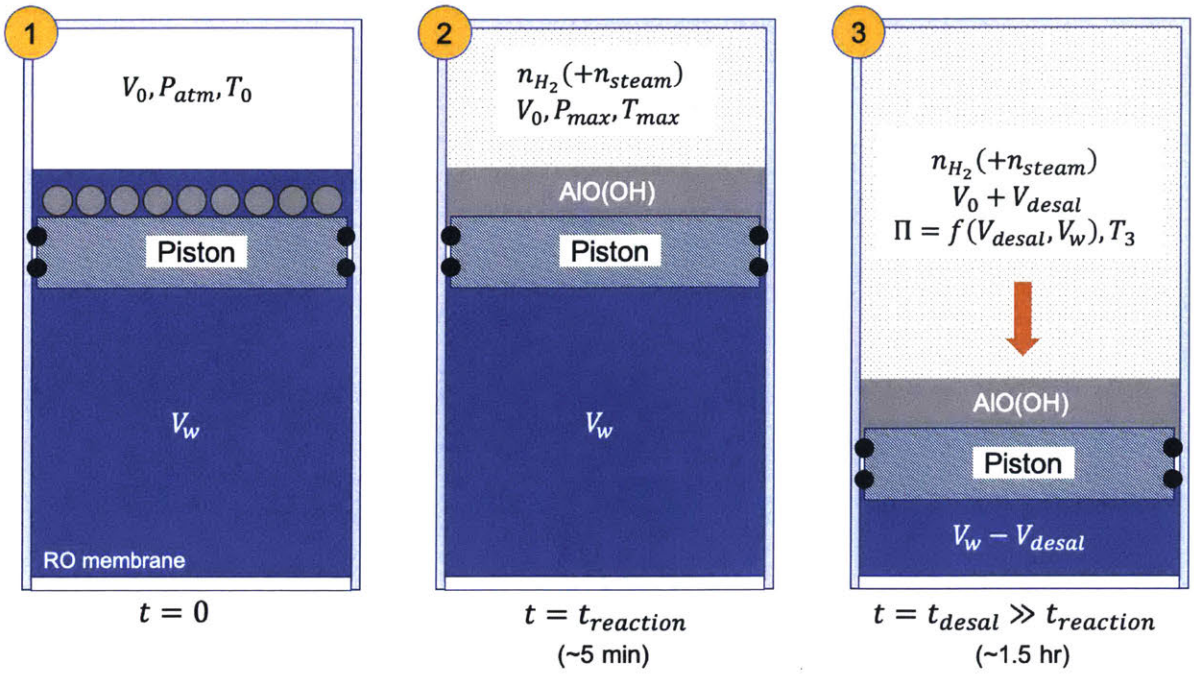

Figure 3-5: Depiction of the three states used in the thermodynamics analysis of the aluminum-powered HDRO process developed here.

data. The result of this assumption is that the height of the piston effectively does not change over the course of the reaction, and thus at State 2 at some time $t_{reaction}$ later, the volume of the top portion of the piston remains at V_0. Because the reaction has completed, however, there are now n_{H_2} moles of hydrogen gas and n_{steam} moles of steam (depending on how well insulated the reactor is), bringing the total system pressure up to P_{max} and the top portion of the piston to a temperature of T_{max}. It assumed throughout this entire process that the temperature of the seawater below the piston remains at T_0. The degree to which steam is produced in this reaction is subsequently explored here in detail. After time $t_{reaction}$, the system pressure, P_{max}, is above the osmotic pressure, $\Pi(t)$, and water begins to permeate through the membrane at the bottom of the piston. Consequently, the volume of the top portion of the piston begins to expand as more and more water is desalinated.

In the last phase of this HDRO process, as more and more water is desalinated, the concentration of solute in the feed solution increases, causing the osmotic pressure to increase over time as well. At the same time, as the volume of the top portion of the piston increases, the pressure of the reaction product gasses decreases. These opposing processes continue as

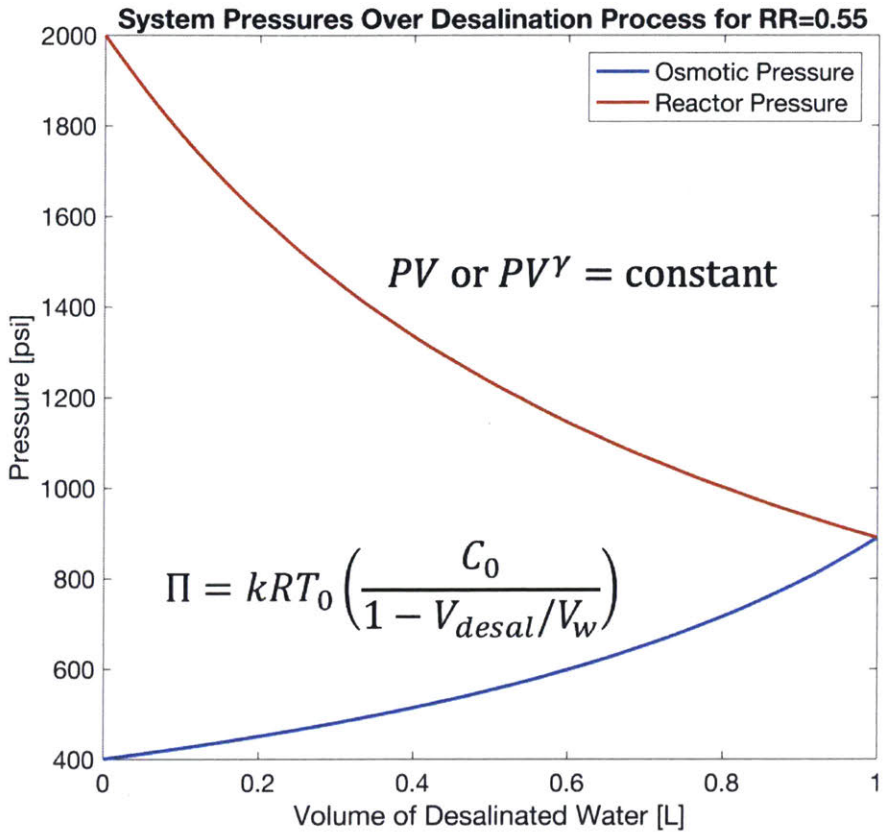

Figure 3-6: Evolution of the system pressure and osmotic pressure for a dead-ended batch desalination process.

shown in Fig. 3-6 until the system pressure equals the osmotic pressure and no more water can be desalinated. This point occurs at time t_{desal} and is labeled here as State 3. At this final state, the top portion of the piston has expanded to a final volume of $V_0 + V_{desal}$, where V_{desal} is the volume of water that permeated through the membrane over the course of this process. The final temperature of the product gasses is T_3.

Strategy for Bounding System Performance

The performance of an aluminum-powered HDRO system is evaluated by bounding the system efficiency based on how well the piston can be thermally insulated. For a lower bound, the piston is assumed to remain at a temperature T_0 throughout the entire process. In this case, the increase in system pressure comes entirely from the increase of gas density that results from the generation of hydrogen. In the maximum efficiency case, the assumption of

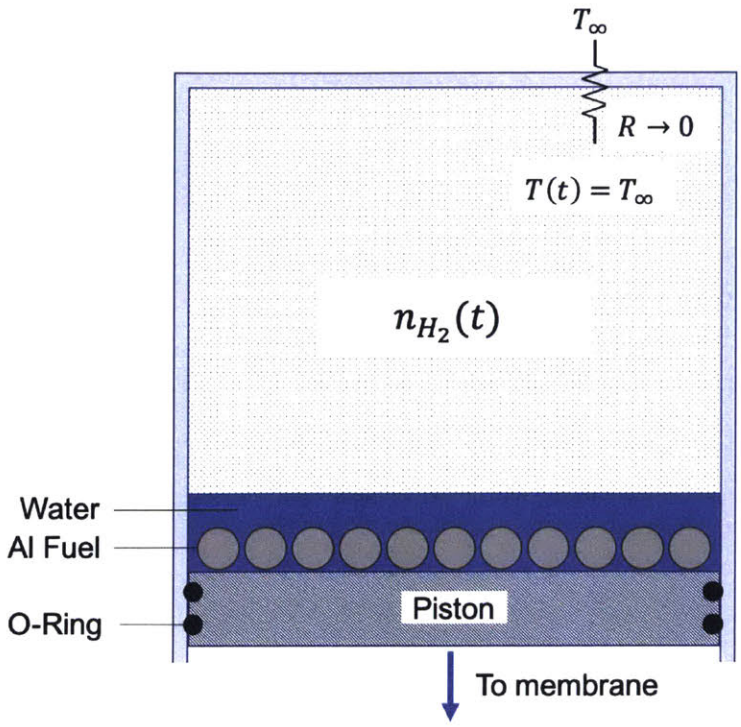

Figure 3-7: Model for the lower HDRO performance bound in which the piston is assumed to be non-insulating.

perfect insulation is not enough to reasonably estimate the performance of a physical system. For this case, we can think of this process as being akin to combustion in an enclosed volume and derive an adiabatic flame temperature equivalent. That is to say, if aluminum and water react precisely stoichiometrically to produce hydrogen in a perfectly thermally insulated (adiabatic) enclosure, the gas would reach temperatures beyond the limits of what most reasonable materials for this application could withstand. As is typically done with internal combustion engines, this process is instead assumed to run "lean", whereby more water is added to the reaction than stoichiometrically required in order to produce some steam as well. This addition reduces the total system efficiency in order to lower the temperature of the reaction products by transferring some reaction enthalpy into the latent heat of water. This loss in temperature, however, is partially balanced by the production of more moles of gas (steam) to generate the pressure required for HDRO. Fewer moles of hydrogen must then be generated to achieve the same pressure, reducing fuel consumption. Both of these performance bounds are explored in detail here.

State	Number of moles of gas	Temperature	Pressure	Upper piston volume
1	0	T_0	P_{atm}	V_0
2	n_{H_2}	T_0	P_{max}	V_0
3	n_{H_2}	T_0	Π	$V_0 + V_{desal}$

Table 3.1: Summary of thermodynamic states for lower efficiency bound HDRO analysis.

3.2.1 Lower Efficiency Bound

For the lower performance bound, the efficiency is assumed to be primarily limited by the poor thermal insulation of the piston housing. In particular, it assumed that any heat release from the aluminum-water reaction is immediately transferred away from the product gas and out into the ambient environment (i.e. $T(t) = T_0 = T_\infty$). For this case, it is additionally assumed that aluminum and water are reacted in a stoichiometric ratio of 2:1, water to aluminum, as given by Eq. 2.2. Finally, because this analysis is performed assuming some physical limitations of a manufacturable system, it is assumed that the pressure cannot exceed some P_{max} over the course of this process. Table 3.1 summarizes the state variables at States 1-3 for the following analysis.

Analysis

To determine how much aluminum fuel is required to drive this process, it is first necessary to derive a relationship between how much aluminum and water can be reacted before the maximum pressure P_{max} is exceeded in State 2. To this end, this pressure relates to the number of moles of hydrogen produced, n_{H_2}, and the initial system temperature and volume by the ideal gas law, given as

$$P_{max} V_0 = n_{H_2} R T_0, \tag{3.4}$$

where R is the ideal gas constant. From the stoichiometry we can relate the number of moles of hydrogen produced to the number of moles of aluminum reacted by

$$n_{H_2} = \frac{3}{2} n_{Al}. \tag{3.5}$$

Combining Equations 3.4 and 3.5 yields a simple closed form expression for the maximum

number of moles of aluminum that can be reacted in this process so as to not exceed the maximum specified pressure, P_{max}:

$$n_{Al} = \frac{2P_{max}V_0}{3RT_0} \tag{3.6}$$

In order to relate this expression to the amount of water that can be desalinated by the aluminum-powered HDRO process, State 3 can be used to determine how the final osmotic pressure relates to how much hydrogen is present in the system. We know from the basic operation of the HDRO process that the desalination process stops when the system pressure drops to equal the osmotic pressure, which is itself a function of how much water has been desalinated. This pressure, Π, can be modelled using the van 't Hoff formula, given generally as

$$\Pi = kCRT, \tag{3.7}$$

where k is the van 't Hoff factor (i) multiplied by the osmotic coefficient (ϕ), which accounts for the dissociation of salt into ions in a real solution (e.g. $k = 0.93 \cdot 2 = 1.86$ for NaCl dissociating into Na^+ and Cl^-), and C is the solute concentration. Because the solute remains in solution throughout the desalination process, the final osmotic pressure can be given as

$$\Pi = kRT_0 \left(\frac{C_0 V_w}{V_w - V_{desal}} \right), \tag{3.8}$$

where C_0 is the initial solute concentration, V_w is the initial feed solution volume, and V_{desal} is the total volume of water desalinated. Alternatively, V_{desal}/V_w can be expressed as a recovery ratio, RR, which is the fraction of water extracted from the initial solution. Using this recovery ratio, Eq. 3.8 can be equivalently expressed as

$$\Pi = kRT_0 \left(\frac{C_0}{1 - RR} \right). \tag{3.9}$$

Finally, the fact that the final system pressure must equal the final osmotic pressure after desalinating a volume of water V_{desal} at State 3 can be expressed using the ideal gas law as

$$\Pi \cdot (V_0 + V_{desal}) = \frac{3}{2} n_{Al} R T_0. \tag{3.10}$$

Plugging Eq. 3.9 into Eq. 3.10 yields an expression for the amount of aluminum required to drive this process given as

$$n_{Al} = \frac{2kC_0V_w(V_0 + V_{desal})}{3(V_w + V_{desal})}. \tag{3.11}$$

Eq. 3.11 can be further simplified, however, since we have an expression for V_0 given by Eq. 3.4. Combining these equations and solving for n_{Al} gives a final expression for the amount of fuel required as

$$n_{Al} = \frac{2kC_0V_wV_{desal}}{3\left(V_w - V_{desal} - \frac{kRT_0C_0V_w}{P_{max}}\right)}, \tag{3.12}$$

or equivalently using RR as

$$n_{Al} = \frac{2kC_0V_{desal}}{3\left(1 - RR - \frac{kRT_0C_0}{P_{max}}\right)}. \tag{3.13}$$

Then the initial volume of the top portion of the piston, V_0, must be

$$V_0 = \frac{3n_{Al}RT_0}{2P_{max}} \tag{3.14}$$

in order for the system pressure to not exceed P_{max} in State 2. The total piston volume, V_T, is consequently given as $V_w + V_0$. We can see from these equations that as the recovery ratio approaches $1 - \frac{kRT_0C_0}{P_{max}}$, the amount of fuel required, and therefore the total system volume, blows up to infinity. On the other end, as the recovery ratio approaches zero, the amount of water required at the outset of the process, V_w, and therefore the total system volume also blows up to infinity. The results of this analysis can be seen in Fig. 3-8 and 3-9.

Sizing and Fuel Consumption Results

This analysis was carried out using MATLAB and these equations were evaluated for a P_{max} of 138 bar and initial salinity of 3.5% (NaCl). The results are presented in Figs. 3-8 and

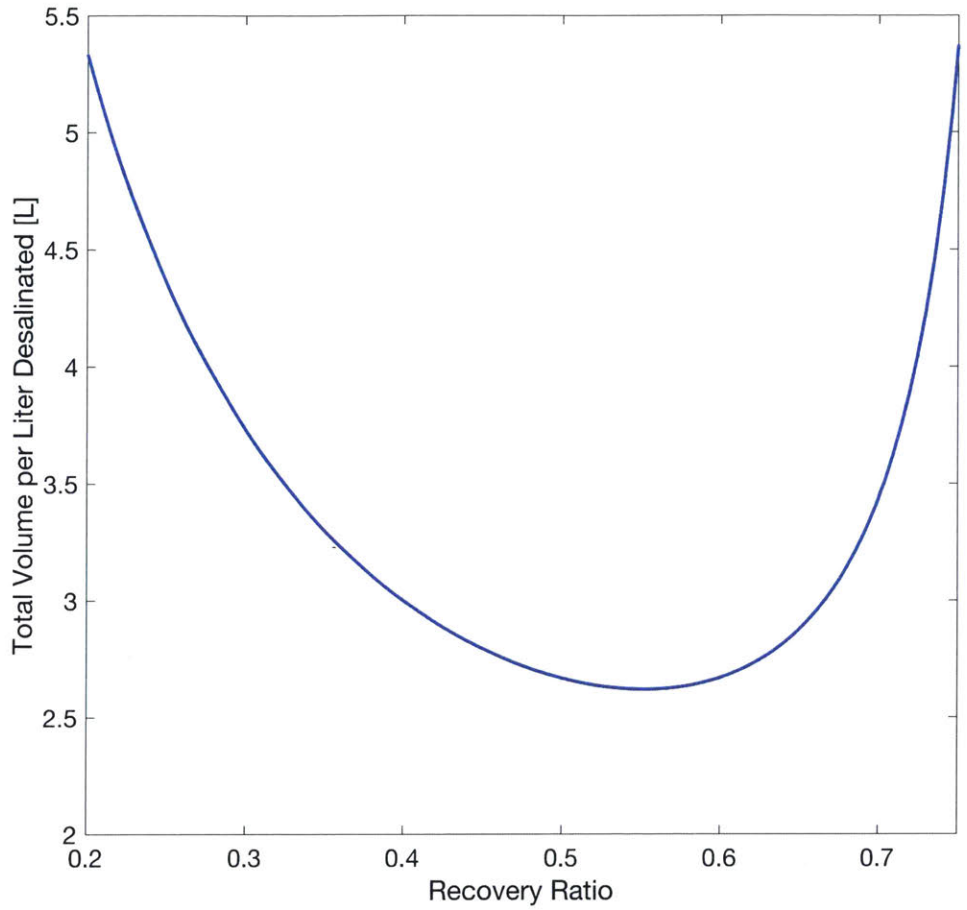

Figure 3-8: Total piston volume per liter 3.5% salinity feed solution desalinated for the lower efficiency bound HDRO model.

3-9, and show the total piston volume and required fuel mass for desalinating 1 liter of water under these conditions. As shown in these figures, both the total piston volume and fuel mass have vertical asymptotes at a recovery ratio of approximately 0.8, indicating that the system cannot be operated for recovery ratios beyond this point.

For this analysis, as shown in Fig. 3-8, the volume of the HDRO system in the poorly insulated case can be minimized by operating at a recovery ratio of 0.55, which would require a total piston volume of 2.6 liters and a fuel consumption of roughly 82 grams of aluminum per liter desalinated. For applications where space is not limited, a larger system running at a lower recovery ratio can significantly reduce fuel consumption, ultimately reaching a value of 33 grams of aluminum per liter desalinated for recovery ratios approach 0.2. The total

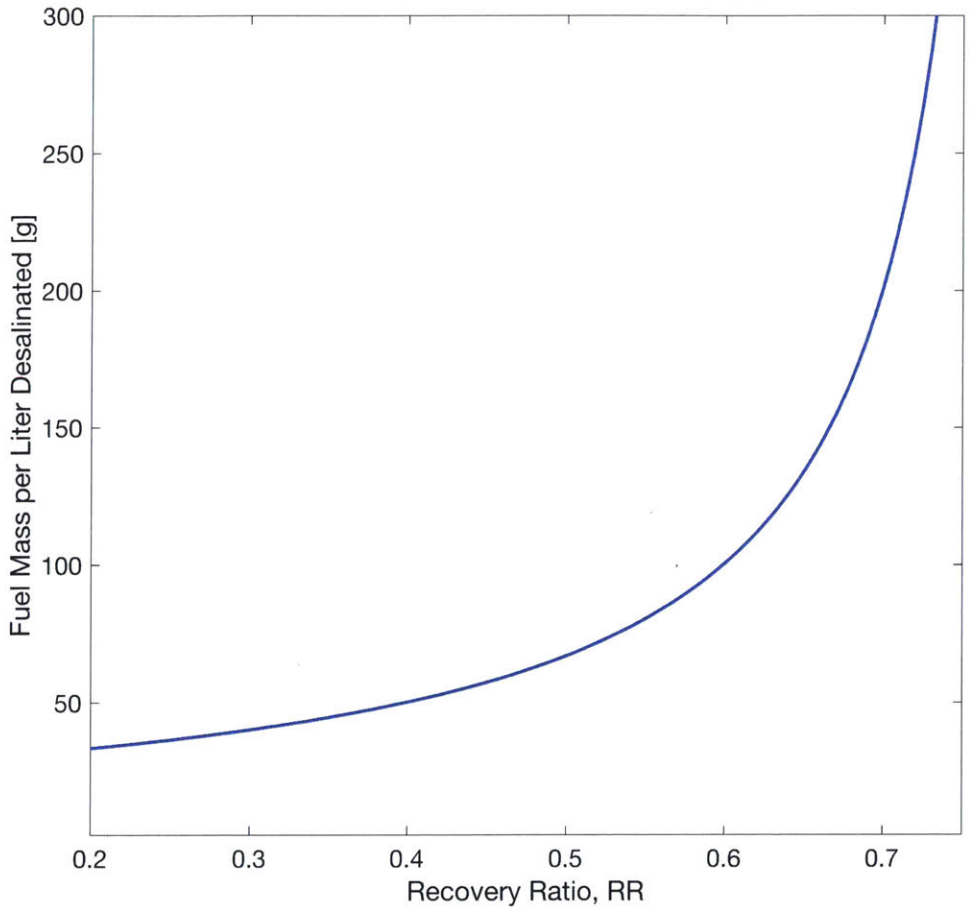

Figure 3-9: Required aluminum fuel mass per liter 3.5% salinity feed solution desalinated for the lower efficiency bound HDRO model.

piston volume at this recovery ratio would be 5.3 liters per liter desalinated.

3.2.2 Upper Efficiency Bound

The analysis for the upper efficiency bound of the aluminum-powered HDRO process is considerably more complex than for the lower efficiency bound case. As previously described, the most optimal adiabatic system would require that the piston materials be able to withstand temperatures on the order of several thousand Kelvin, well above the melting point of steel and most other materials that could reasonably be used to manufacture this system. Consequently, it is assumed that this system must instead run "lean", meaning that more water than is stoichiometrically required is added to the reaction to absorb some of the thermal energy as latent heat of water in the production of steam. In this case, the piston is still assumed to be perfectly adiabatic and that the thermal energy released as the enthalpy of reaction for the aluminum-water reaction is transferred solely to the hydrogen, steam, and aluminum oxyhydroxide products. Fig. 3-10 shows a graphical depiction of this model, and Table 3.2 summarizes the state variables used for each of the States 1-3 used to describe this process. For this analysis, the process again stops once the system pressure reaches the osmotic pressure.

Key Assumptions

For this mode of operation, the production of steam increases the density of the product gasses, thereby reducing the amount of fuel required to reach the maximum pressure, P_{max}, which again is set by the limitations of the materials used to manufacture the HDRO system. In order to operate most fuel efficiently in this regime, no excess liquid water should be present in the system, as thermal energy transferred to increase the sensible heat of the solid or liquid phases does not contribute to increasing the pressure of the system and in turn the amount of water that can ultimately be desalinated. Therefore, the following analysis proceeds under several key assumptions:

1. The piston is perfectly insulated and all thermal energy remains within a control volume encompassing just the aluminum-water reaction products.

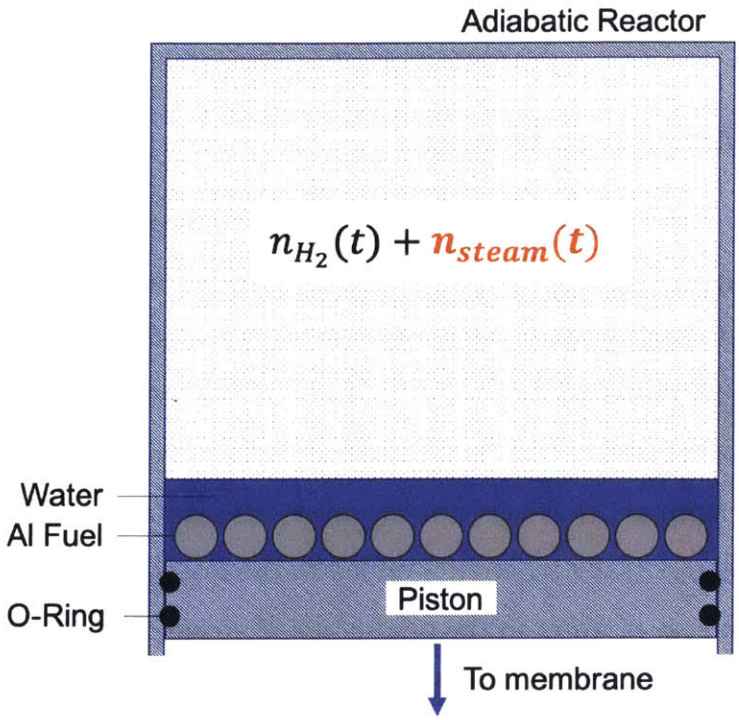

Figure 3-10: Model for the upper HDRO performance bound in which the piston is assumed to be perfectly adiabatic.

2. Excess water is added to the reaction to generate super-heated steam at State 2.

3. The piston expands adiabatically until just before the steam condenses at State 3 and at no point before does the steam condense (see Fig. 3-11).

4. The initial volume of air or other inert gasses in the top portion of the piston at the beginning of the process is negligible.

Analysis

Using the same thermodynamic states shown in Fig. 3-5, the analysis for determining the amount of fuel required and the total system volume for desalinating a volume, V_{desal}, of seawater at some initial concentration, C_0, at some recovery ratio, RR, proceeds as follows. First, the assumption that the steam just begins to condense at State 3 can be stated simply using the Antoine Equation as

$$\log_{10} P_{sat}(T_3) = A - \frac{B}{C + T_3}, \tag{3.15}$$

State	Number of moles of gas	Temperature	Pressure	Upper piston volume
1	0	T_0	P_{atm}	V_0
2	$n_{H_2} + n_{steam}$	T_{max}	P_{max}	V_0
3	$n_{H_2} + n_{steam}$	T_3	Π	$V_0 + V_{desal}$

Table 3.2: Summary of thermodynamic states for upper efficiency bound HDRO analysis.

where T_3 is the final gas temperature at State 3, P_{sat} is the saturation pressure of water, and A, B, and C are curve fit parameters, which are tabulated for water over a range of temperatures by [15] and [4]. This equation states that partial pressure of steam in the system reaches its saturation pressure at the final temperature in State 3. If the steam cools below this point via additional expansion of the piston, the steam will condense and the entire process loses efficiency. This constraint is shown graphically in the T-S diagram for this process in Fig. 3-11. Consequently, this final temperature drives all other states of this process.

Because the number of moles of steam present in the system, n_{steam}, is assumed to remain constant over the HDRO process, it can therefore be given by the ideal gas law as

$$n_{steam} = \frac{P_{sat}(T_3) \cdot (V_0 + V_{desal})}{RT_3}. \tag{3.16}$$

Assuming adiabatic expansion of the piston, T_3 can be related back to T_{max}, which is the maximum system temperature at State 2, P_{max}, and the final osmotic pressure at State 3, Π, by the following equation:

$$T_3 = T_{max}\left(\frac{P_{max}}{\Pi}\right)^{\frac{1-\gamma}{\gamma}}, \tag{3.17}$$

where γ is the molar averaged heat capacity ratio for the product gasses, and again, the osmotic pressure is modelled using the van 't Hoff formula given by Eq. 3.8.

As before, the number of moles of aluminum required to produce hydrogen gas at State 3 at a partial pressure of P_{H_2} can be given by the ideal gas law as

$$n_{Al} = \frac{2P_{H_2}V_3}{3RT_3}, \tag{3.18}$$

but we also know that at State 3, the osmotic pressure must equal the sum of the partial

pressures of hydrogen, P_{H_2}, and steam, $P_{sat}(T_3)$, yielding the relation

$$n_{Al} = \frac{2\left(\Pi - P_{sat}(T_3)\right)\left(V_0 + V_{desal}\right)}{3RT_3}. \tag{3.19}$$

The initial volume of the top portion of the piston, V_0, is then given by

$$V_0 = \frac{\left(\frac{3}{2}n_{Al} + n_{steam}\right) RT_{max}}{P_{max}}, \tag{3.20}$$

so as to not exceed P_{max} in State 2. In these equations, T_{max}, and thus T_3, are still unknown, and to solve for these variables, an energy balance across States 1 and 2 must be applied to relate the enthalpy of reaction, Δh_{rxn}, for the aluminum-water reaction to the temperature of the system at State 2, T_{max}. A First Law analysis can be applied to the control volume encompassing only the reactants and subsequent products to relate the change in internal energy to the change in enthalpy and in the product of pressure times volume by

$$\Delta E = \Delta H - \Delta(PV) = 0. \tag{3.21}$$

Because no work is done on or by the contents of the control volume between States 1 and 2, and because the piston is assumed adiabatic throughout this process, no energy is exchanged with the environment, and thus, there is no change in internal energy between these states. ΔH can be expanded to include the contributions from the different reactant and product species as

$$\sum_{i=1}^{j} n_i h_i(T_{max}) - \sum_{i=1}^{k} n_i h_i^0 - (P_{max} - P_{atm})V_0 = 0, \tag{3.22}$$

where j is the number of product product species at temperature T_{max} in State 2 and k is the number of reactant species at initial temperature T_0. Here h_i^0 indicates that the enthalpy per mole is taken at a reference temperature of T_0. $\Delta(PV)$ is also expanded here to show the change in pressure and the fact that the volume, V_0, remains constant across these states.

The remaining unknowns in this analysis are the individual enthalpy values, h_i, for the product and reactant species that participate in the aluminum water reaction. These values depend on temperature, material, and phase of the material and are typically non-linear. To

approximate these values, NASA provides a comprehensive list of curve fit equations for a wide range of species in their various typically encountered phases. The equations are each of the form

$$\frac{h_i(T)}{RT} = -a_1 T^{-2} + a_2 \frac{\log T}{T} + a_3 + a_4 \frac{T}{2} + a_5 \frac{T^2}{3} + a_6 \frac{T^3}{4} + a_7 \frac{T^4}{5} + \frac{b_1}{T}, \tag{3.23}$$

where T is the species temperature and constants a_1-a_7 and b_1 are curve-fit parameters provided in [17]. For this analysis, these parameters are given for crystalline aluminum, liquid water, steam, and hydrogen gas. Data for aqueous aluminum oxyhydroxide, however, were not provided by these NASA thermodynamics tables, and instead data from [8] were used to curve fit the following fourth-order polynomial:

$$h_{AlOOH}(T) = -1.044 \cdot 10^{-6} T^4 + 1.82 \cdot 10^{-3} T^3 - 1.133 T^2 + 294.3T - 1023 \cdot 10^3, \tag{3.24}$$

which provides the enthalpy for aluminum oxyhydroxide at temperature T in units of J/mol.

Model Implementation

The culmination of this analysis is a series of non-linear equations which can be solved numerically for the amount of aluminum required, n_{Al}, to desalinate a volume, V_{desal}, of water of some initial known concentration, C_0, at some recovery ratio, RR. The maximum pressure of the system at State 2, P_{max}, is applied as a constraint on the system, and therefore both the initial volume of the top portion of the piston, V_0, and the temperature at State 2, T_{max}, can be solved for as well. This numerical analysis is performed using MATLAB and its built-in `solve()` function set to only accept real solutions. To reduce computation time, bounds for the solutions to each variable are also provided. The code iterates over a range of recovery ratios spaced logarithmically between 0.1 and 0.9 and stores the solution to each variable at each intermediate step. On occasion, specific values of RR cause the solver to hang and timeout. To remedy this issue, RR is incremented by a small amount and the numerical solver is called again. This process repeats several times until a solution is found.

The solutions to the state variables for this cycle can be visualized as in Fig. 3-11, which

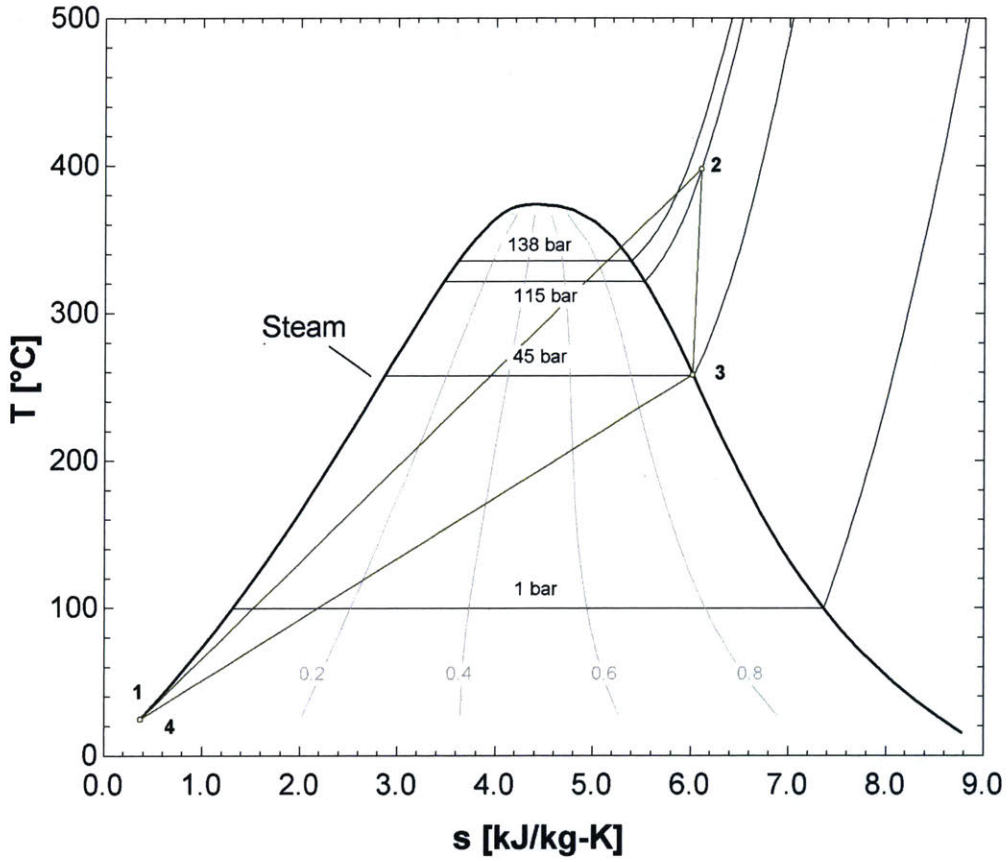

Figure 3-11: T-S diagram for HDRO process running at recovery ratio of 0.5. This cycle is only just the steam within the piston. The desalination occurs between States 2 and 3 here.

depicts the T-S diagram for the water within the system during this complete cycle, as well as the vapor dome for steam. This diagram shows the initial evaporation, pressurization, and super-heating between States 1 and 2, the adiabatic expansion of the piston to desalinate water between States 2 and 3, and finally resetting the system between States 3 and 4 (i.e. State 4 is equivalent to State 1). This particular diagram is shown for a single recovery ratio of 0.5, but it illustrates the basic thermodynamic process behind HDRO. It is also interesting to note here that the saturation pressure of steam at State 2 is 115 bar, which is a large fraction of the total system pressure of 138 bar, indicating that the majority of the pressurization comes from the generation of steam. The added pressure from producing moles of hydrogen is nearly negligible for this upper efficiency bound case, and therefore any other source of heat that can be reasonably supplied would exhibit similar performance under

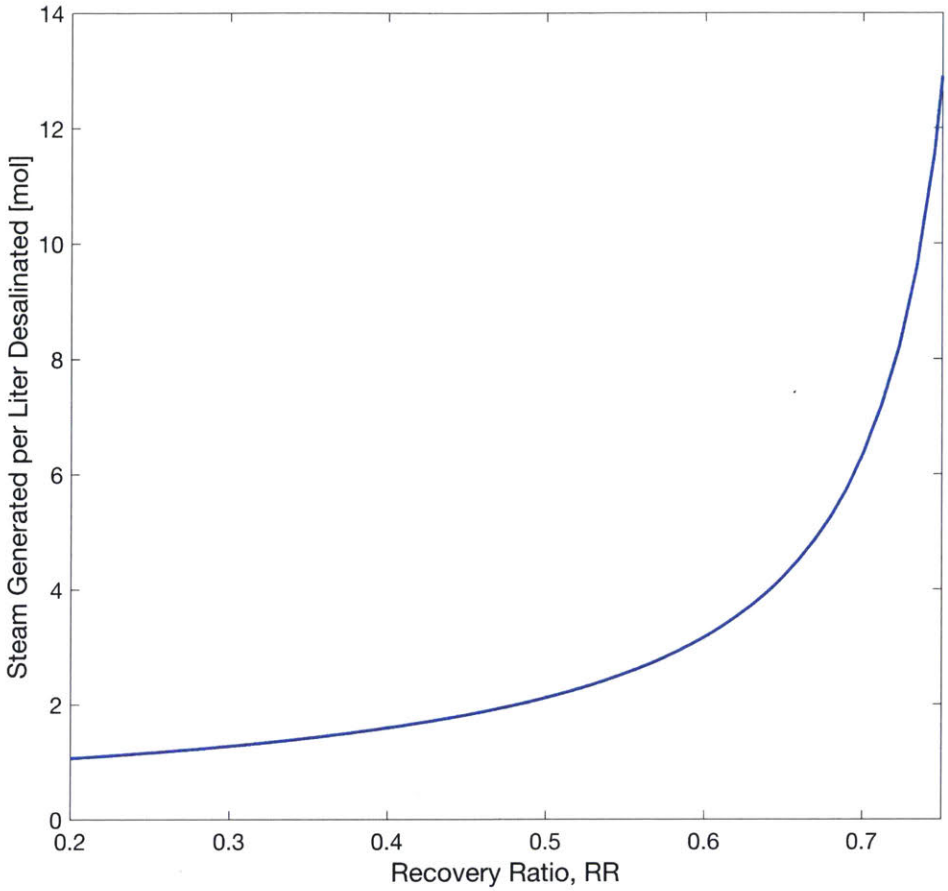

Figure 3-12: Required moles of steam generated per liter of water desalinated as a function of recovery ratio for the upper efficiency bound HDRO model.

the same assumptions. To contrast this, for the lower efficiency bound case, the hydrogen generation is responsible for the all of the pressurization, indicating that the performance is highly tied to this particular aluminum-water reaction heat source for a poorly insulated system.

Maximum System Temperature

For this model of the HDRO process, even though extra water is added to the reaction in order to absorb some of the thermal energy released, the system can still reach temperatures above 430 °C for low recovery ratios, as shown in Fig. 3-13. Also shown in this plot of maximum reactor temperature as a function of recovery ratio, is that the temperature increases as the

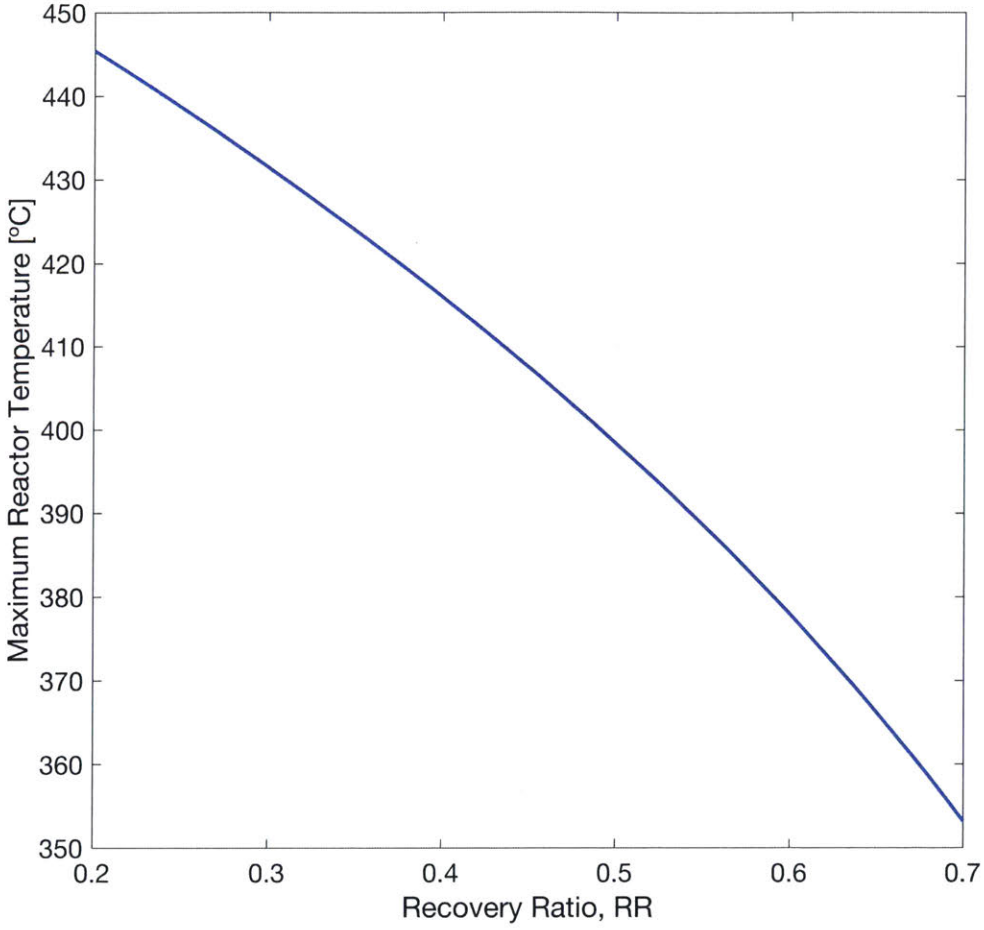

Figure 3-13: Maximum temperature, T_{max}, at State 2 as a function of recovery ratio for the upper efficiency bound HDRO model.

recovery ratio decreases. While seemingly counter-intuitive, this phenomenon is explained mathematically by understanding that for low recovery ratios, the final osmotic pressure increases significantly over the course of HDRO process. Rearranging Equation 3.17 yields

$$T_{max} = T_3 \left(\frac{\Pi}{P_{max}} \right)^{\frac{1-\gamma}{\gamma}}, \tag{3.25}$$

where where γ is the heat capacity ratio and is greater than one for both hydrogen and steam (1.41 and 1.33 respectively). Therefore, the exponent in this equation is negative for this process, resulting in an inverse relationship between final osmotic pressure and maximum temperature.

Intuitively, as the recovery ratio increases and the final osmotic pressure increases accordingly, the total change in system pressure of the piston between States 2 and 3 decreases for a fixed P_{max} at State 2. For a smaller change in pressure, more steam can be generated without it condensing before reaching State 3. Fig. 3-12 shows the amount of steam required to drive this process as a function of recovery ratio, confirming this hypothesis. More generated steam results in more thermal energy being removed from the system as latent heat, thereby reducing the overall system temperature. This maximum temperature must be considered when designing a physical system using HDRO as its underlying mechanism. For an imperfectly insulated piston, a trade-off exists between operating the system at less efficient higher recovery ratios and lower temperatures to reduce rate of heat loss and operating at more efficient lower recovery ratios and higher temperatures, for which the rate of heat transfer out of the system will increase. Transient models of this phenomenon must be developed in order to determine the most efficient operating point.

Sizing and Fuel Consumption Results

The results for the total piston volume and aluminum fuel mass required for desalinating 1 liter of 3.5% salinity seawater is shown in Figs. 3-14 and 3-15 respectively. Again, a maximum system pressure of 138 bar was used for this computation. As is the case for the lower efficiency bound analysis, there is a clear minimum total system volume that arises from the balance between adding extra water initially to achieve a low recovery ratio and

increasing the reaction portion of the piston to store PV energy and avoid exceeding P_{max}. Similar to the lower efficiency bound analysis, for recovery ratios near 0.8, the solution for the total piston volume becomes undefined, and for recovery ratios beyond 0.8, the solutions become negative, indicating that for this system, it is not possible to operate a recovery ratios beyond 0.8 under the assumptions provided at the outset of this analysis.

In terms of fuel consumption, as Fig. 3-15 shows, the required quantity of aluminum required to drive the HDRO process is significantly less in this case than for the lower efficiency bound as expected. For the upper efficiency bound analysis, the amount of aluminum required per liter of 3.5% seawater desalinated approaches 3.9 g at a recovery ratio of 0.2, providing an upper bound for the expected performance of an HDRO process. For a recovery ratio of 0.5, this increases to 7.5 g Al per liter desalinated, which is roughly half the mass of an empty 12 oz aluminum soda can for physical reference.

3.2.3 Comparing Efficiency Bounds

It is possible to define numerous efficiency measures for desalination processes. A second law efficiency, for example, might compare the work done by the piston to the least work required to desalinate the equivalent quantity of water. A first law efficiency could similarly be used to compare the work performed by the piston over the HDRO process to the heat released by the aluminum-water reaction. While both are useful metrics for optimizing the HDRO process itself, it is important to first understand how this process compares to other thermally-driven desalination processes in order to determine whether this technology is worth pursuing above others. To this end, a standard performance ratio, PR, is defined as

$$PR = \frac{\rho_w V_{desal} h_{fg}(T_0)}{n_{Al} \Delta h_{rxn}}, \tag{3.26}$$

which relates the latent heat of the water desalinated to the thermal energy supplied to the process (i.e. the enthalpy of reaction for the aluminum-water reaction). In other words, the performance ratio compares the fuel efficiency to that of simply boiling off the equivalent quantity of water without recapturing any of the latent heat. A performance ratio of 5, for example, indicates that a process can desalinate 5 times more water than single-state

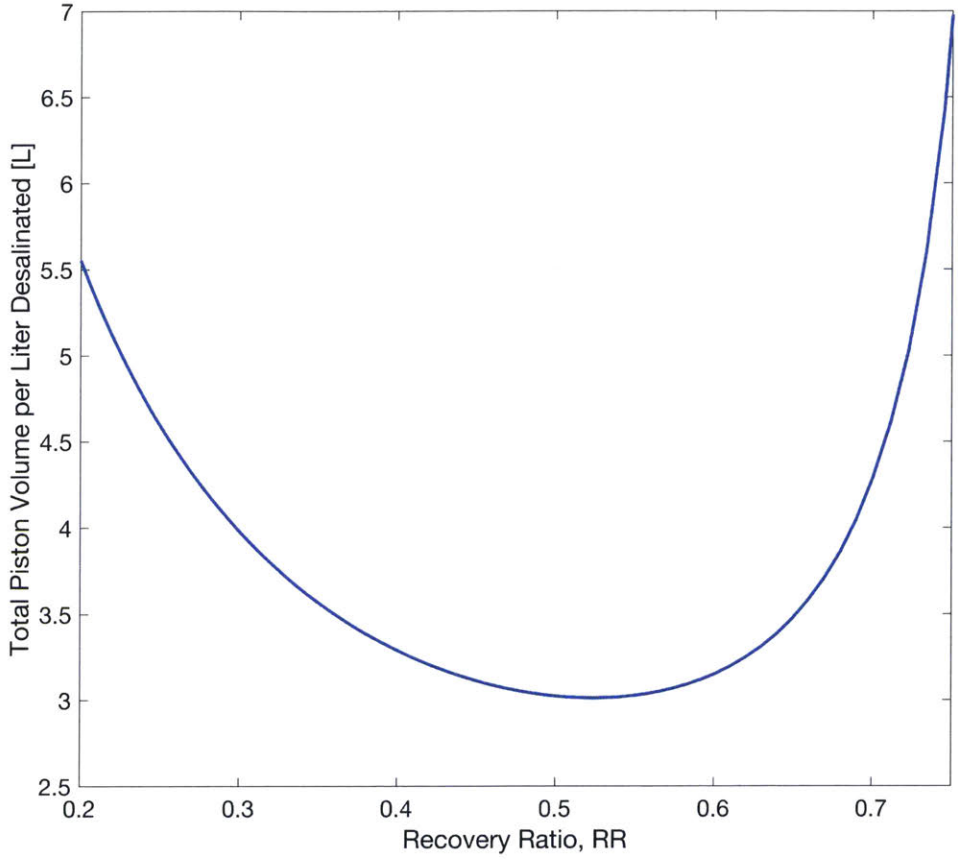

Figure 3-14: Total piston volume per liter 3.5% salinity feed solution desalinated for the upper efficiency bound HDRO model.

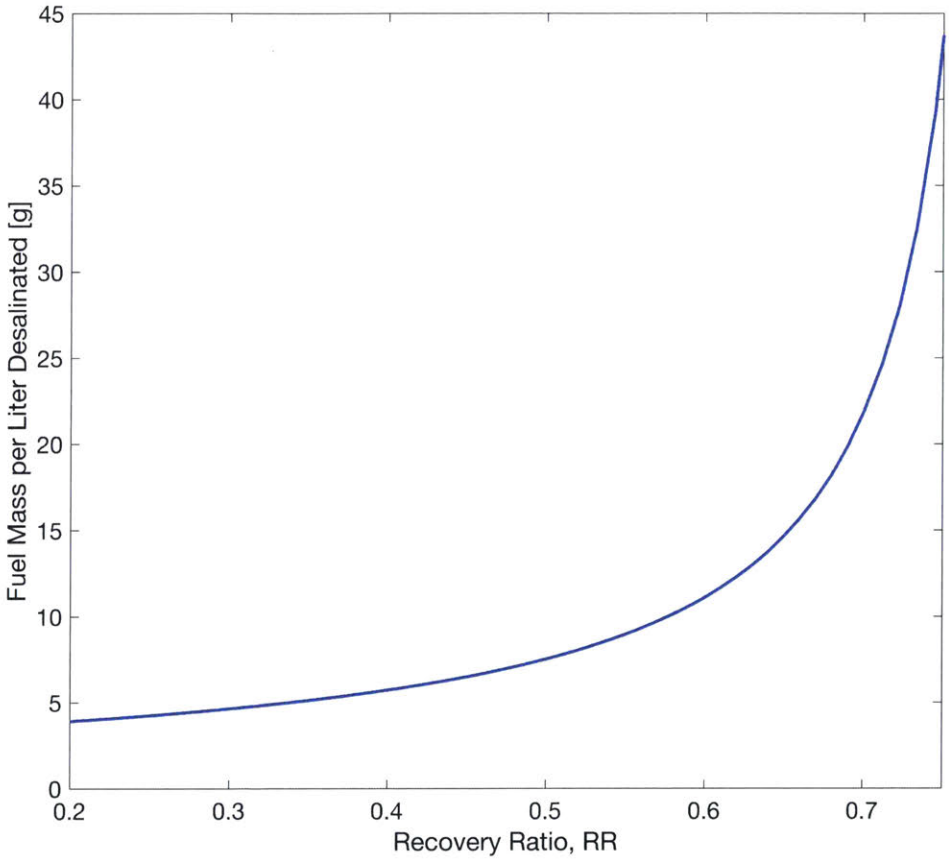

Figure 3-15: Required aluminum fuel mass per liter 3.5% salinity feed solution desalinated for the upper efficiency bound HDRO model.

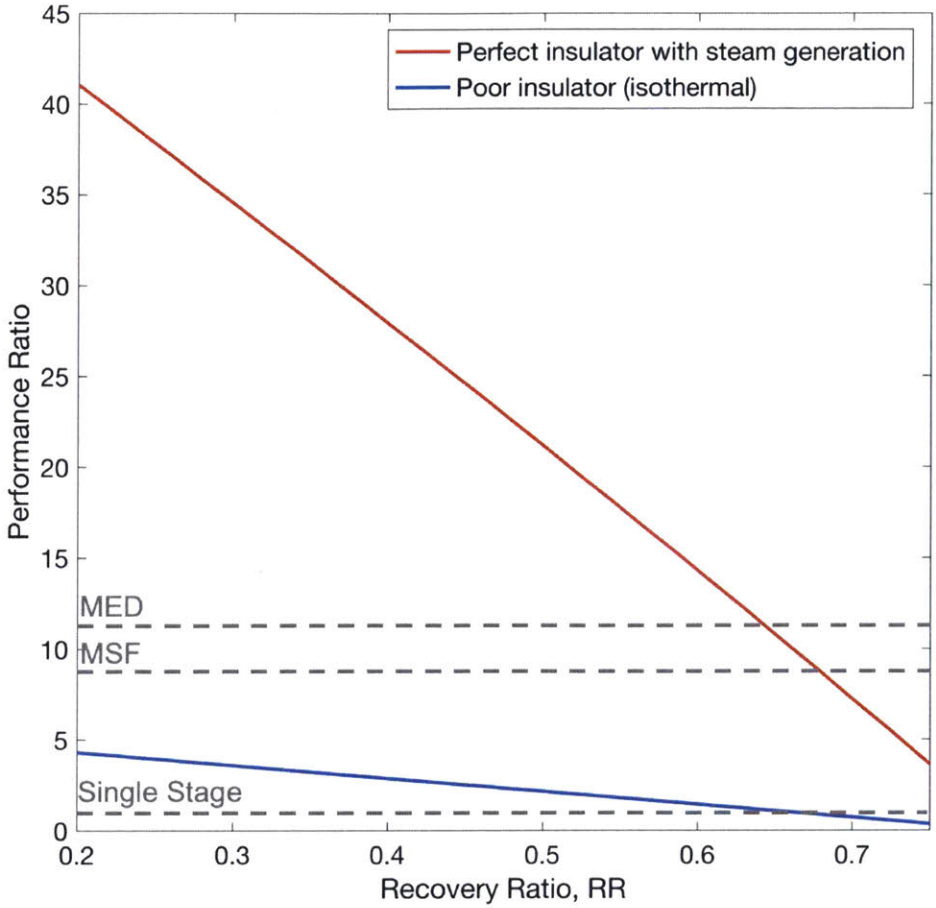

Figure 3-16: Performance ratio bounds for HDRO shown in comparison to single stage evaporation, MED, and MSF.

evaporation for the same amount of thermal energy input.

The performance ratio for HDRO is computed for both the upper and lower efficiency analyses as bounds for an actual system performance ratio, and the results are shown in Fig. 3-16. The performance ratio is naturally a function of recovery ratio and is shown as approximately linear here due to the effective logarithmic scaling inherent to presenting the recovery ratio in this manner. For low recovery ratios, this value approaches 41 for the most optimal case and 4.3 for the least optimal case presented here. To compare this process to other thermally-driven desalination processes, the performance ratios for single stage evaporation, MED, and MSF are shown in Fig. 3-16 as well.

Compared to single stage evaporation, even in the case where most of the thermal energy released in the aluminum-water reaction is transferred out of the piston, HDRO is several

times more efficient over a wide range of recovery ratios. At a moderate recovery ratio of 0.5, HDRO can desalinate between 2 and 21 times more water for the same heat input, depending on factors like the degree to which the HDRO piston can be thermally insulated, for example. What is also promising about these results, is that HDRO also has the potential to be significantly more fuel efficient than state-of-the-art MED and MSF plants, which currently achieve performance ratios in the range of 8-12 [20]. This result shows that not only is HDRO viable for small scale disaster relief and preparedness applications, but may also be a viable alternative to large scale, thermally-driven desalination plants. It is also important to note that this analysis assumed an initial water salinity of 3.5%, so for brackish water with a lower initial salinity, these performance ratios increase accordingly.

3.2.4 Model Limitations

In addition to the previously listed assumptions, a number of other factors were not considered in this analysis. First, it was assumed that there were no energy losses associated with added pressure drops across the RO membrane itself. These membranes can develop salt scale and can foul, creating added frictional losses that would contribute to a larger pressure drop than is accounted for in this analysis. Work by [9] showed that these contributions may not be negligible for certain configurations. Second, concentration polarization (CP), a phenomenon by which the local osmotic at the feed-side surface of the RO membrane increases as a function of the permeation rate, was assumed to be negligible due to slow desalination rates. In reality, a practical HDRO system would need a reasonably high permeation rate, and thus CP may be a non-negligible source of loss as well. Future work will need to model these dynamic phenomena to provide more accurate bounds for the performance of HDRO.

3.3 HDRO Sizing for Different Operating Constraints

The numerous constraints placed on a given desalination system vary widely between applications. Personal-scale water generators for first responders, life boats, and other disaster relief applications, for example, require compact, easily transportable systems, necessitating that total system volume be minimized. For larger scale permanent desalination plants using

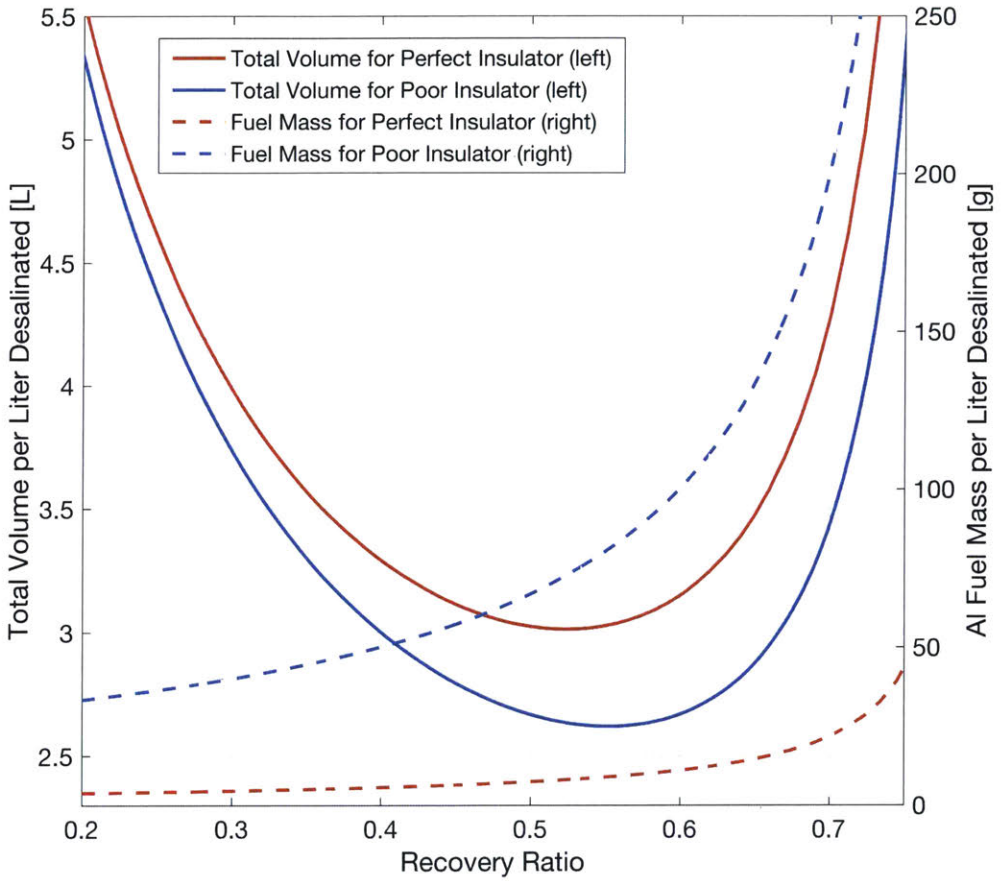

Figure 3-17: Bounds for the required piston volume and aluminum fuel mass per liter of 3.5% salinity water desalinated as a function of recovery ratio. The maximum operating pressure is 138 bar here.

HDRO, fuel efficiency might instead be the driving constraint. Consequently, an engineer designing a system that uses HDRO as its underlying operating mechanism must know how to scale the device according to these different use-case constraints and the physical limitations of system materials, geometries, and manufacturing processes. The plot shown in Fig. 3-17 provides an example of a tool for engineers to use in order to gain a sense for how system volume and fuel consumption scale with recovery ratio for a fixed initial salinity and maximum operating pressure. In particular, this type of plot highlights the trade-off between total system volume and required fuel mass at each recovery ratio. Minimizing fuel consumption, for example, results in a much larger system, and minimizing the volume requires more aluminum be consumed for the same amount of water output. This same plot can be generated for a range of initial water salinities and maximum operating pressures as well. Understanding the balance between these parameters is critical in designing an HDRO system that minimizes capital costs or whatever other quantity is of interest.

3.4 Experimental Validation

3.4.1 Prototype Design

A prototype HDRO system was designed and tested for this research in order to prove out the basic operating principles behind this desalination approach. Figures 3-1 and 3-18 show the test setup used for these experiments. This apparatus simply consists of an insulated piston that is capped on one end and open to a semipermeable membrane housed in a high-pressure membrane assembly on the other. The membrane assembly outputs the desalinated water into a graduated collection tube directly for measurement.

Piston

The custom piston housing is comprised of 1-inch outer diameter 316 stainless steel tubing with a wall thickness of 0.12 inches. Swagelok tube fittings are used to connect to this piston housing on either side. It is important to note here that the Swagelok fittings intentionally deform the tube slightly during their installation, restricting the motion of the piston near

the fittings at the ends of the tube; however, for all recovery ratios of interest here, the piston remains far enough from these deformed regions to be affected by this issue. The piston housing is thermally insulated using 1.5-inch thick fiberglass insulation with an R value of 6.5. A piston manufactured from acetal separates the aluminum-water reaction in the top portion of the tube from the input seawater in the bottom portion. Two neoprene O-rings are used to create a gas-tight seal around the piston during operation. The solubility of hydrogen in water is relatively low, and therefore the primary purpose of this seal is instead to retain as much thermal energy as possible in the reaction portion of the tube during the desalination process. The O-ring grooves are sized for the nominal internal diameter of the tube, and therefore inserting the piston requires some force during installation due to the aforementioned issue with the Swagelok fittings deforming the tube on either end. For the configuration used here, the O-rings were able to sufficiently compress to make it past the deformed regions.

Saltwater Line

For the saltwater line in this prototype, 0.5-inch outer diameter 317 stainless steel tubing connects the bottom of the piston housing to the inlet of the membrane assembly via several additional Swagelok connections. A tee placed directly below the membrane assembly adds an extra inch of tubing below the membrane housing and acts as both a port for filling the system with saltwater at the outset of each test and also as a sediment trap to reduce the risk of small debris being carried into the membrane. Given its displacement from the hot reaction portion of the piston and the fact that it is desirable to keep the water being desalinated at as low a temperature as possible to reduce the osmotic pressure (see Eq. 3.7), it was decided that the tubing connecting the piston and membrane assembly would not be insulated for this prototype.

The membrane assembly itself consists of an off-the-shelf high pressure filter holder from Millipore Sigma (XX4504700) sized to hold 47 mm diameter membranes. This assembly, shown in Fig. 3-19, is manufactured from 316 stainless steel and is rated for inlet pressures of 689 bar, well above the burst pressure of the piston housing tube. Therefore, the maximum system operating pressure is set to 138 bar in order to achieve a 1.5x safety factor (after

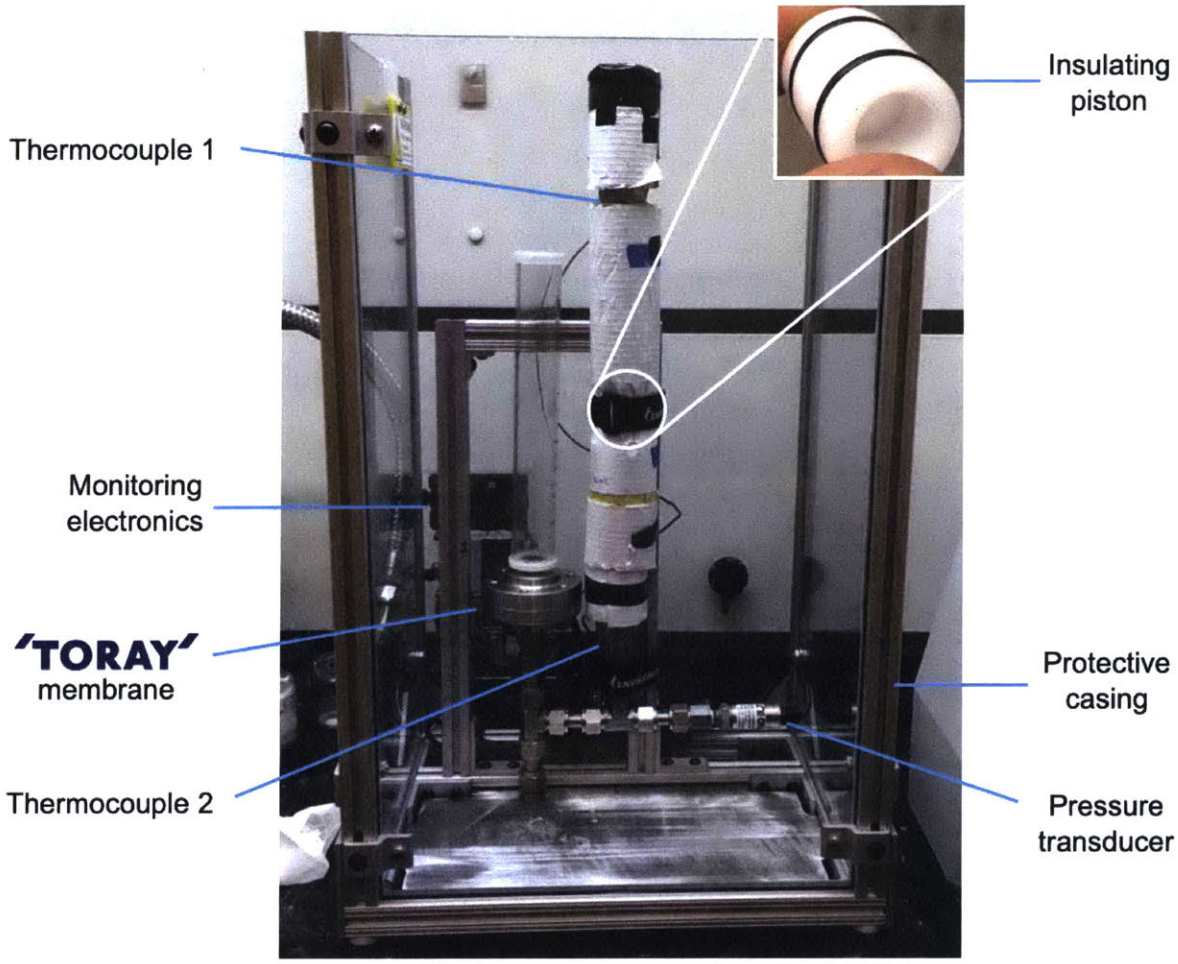

Figure 3-18: HDRO prototype system using stainless steel tubing and a 47mm diameter polyamide membrane.

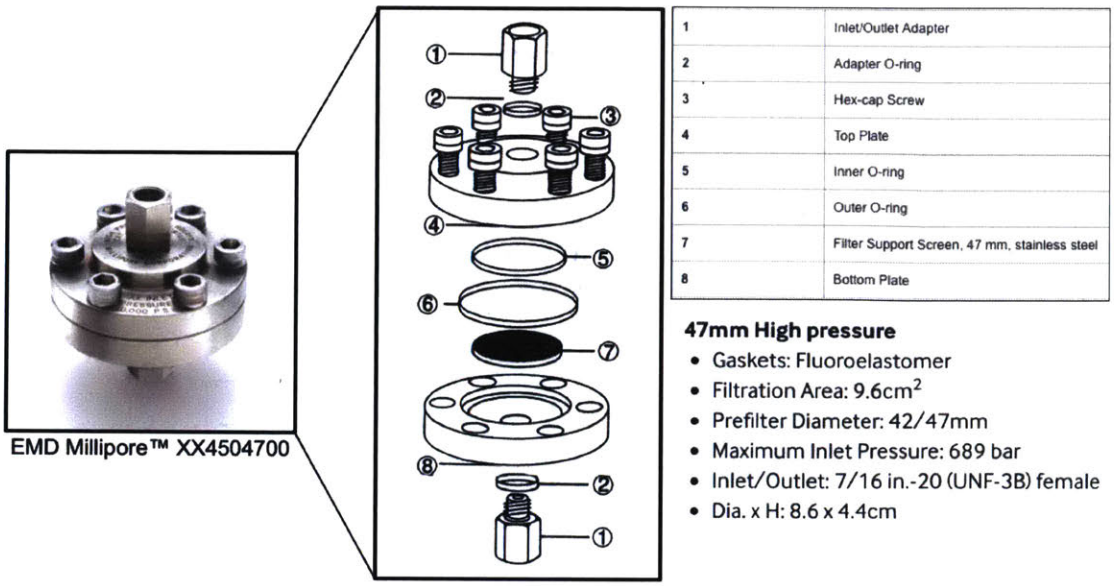

Figure 3-19: HDRO prototype membrane assembly [Millipore Sigma].

derating for the expected system temperatures). As an added precaution, the entire HDRO prototype is placed within a 0.5-inch thick walled polycarbonate case held together using 1-inch 80/20 extrusions.

Sensors and Data Collection

This test apparatus is also outfitted with a number of sensors and components for providing real-time visual feedback to the user. First, the system pressure is measured using an Omega PX309 pressure transducer connected via a Swagelok tee fitting directly below the piston housing. This pressure transducer is sized for 0-3000 psi range and outputs an analog voltage, which is read by the Arduino UNO shown in Fig. 3-21. Second, as shown in Fig. 3-18, two K-type thermocouples are used to measure the temperature in both the top and bottom portions of the piston. Adafruit thermocouple amplifier breakout boards are used to read the thermocouples and transmit the data to the Arduino UNO. The schematic shown in Fig. 3-20 summarizes these connections.

To record and transmit the sensor telemetry to the user, the Arduino microcontroller reads and serializes the data coming from the various sensors in this system. These values are then written as a comma-separated ASCII string to a Raspberry Pi 3 Model B over

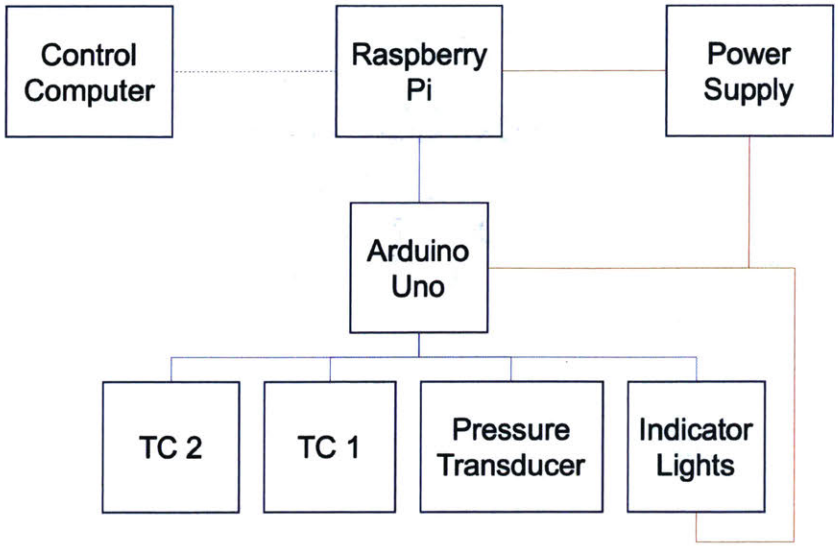

Figure 3-20: Electronics schematic for the HDRO prototype system.

serial. The Raspberry Pi running a standard Raspian Linux distribution stores this data locally, enabling the experiment operator to copy the data to external storage later or query the data file directly. This topology allows for a flexible sensor layout, real-time synchronous data collection, and benefits greatly from the usability of the Linux file system. Finally, in order to avoid needing to bring a monitor into the fume hood, all user-end interactions with the Raspberry Pi are performed remotely via SSH over Wi-Fi.

Operator Feedback

In addition to data collection, this prototype also supports hardware for displaying crucial state information to the user during experimental operations. In particular, because this system intentionally generates high-temperature and high-pressure hydrogen, it is necessary to indicate to the user when the system is "live" so the proper precautions can be made to ensure operator safety. To this end, rows of individually addressable LEDs line the vertical edges of the front face of the protective polycarbonate case. As shown in Fig. 3-22, the height and color of the LED strips are used to visually convey the internal pressure of the system. The red lights indicate that the maximum pressure of 138 bar has been reached. These LED strips can also be used to show the internal temperatures at various points in the system and switch between the different "scenes" in order to convey different information

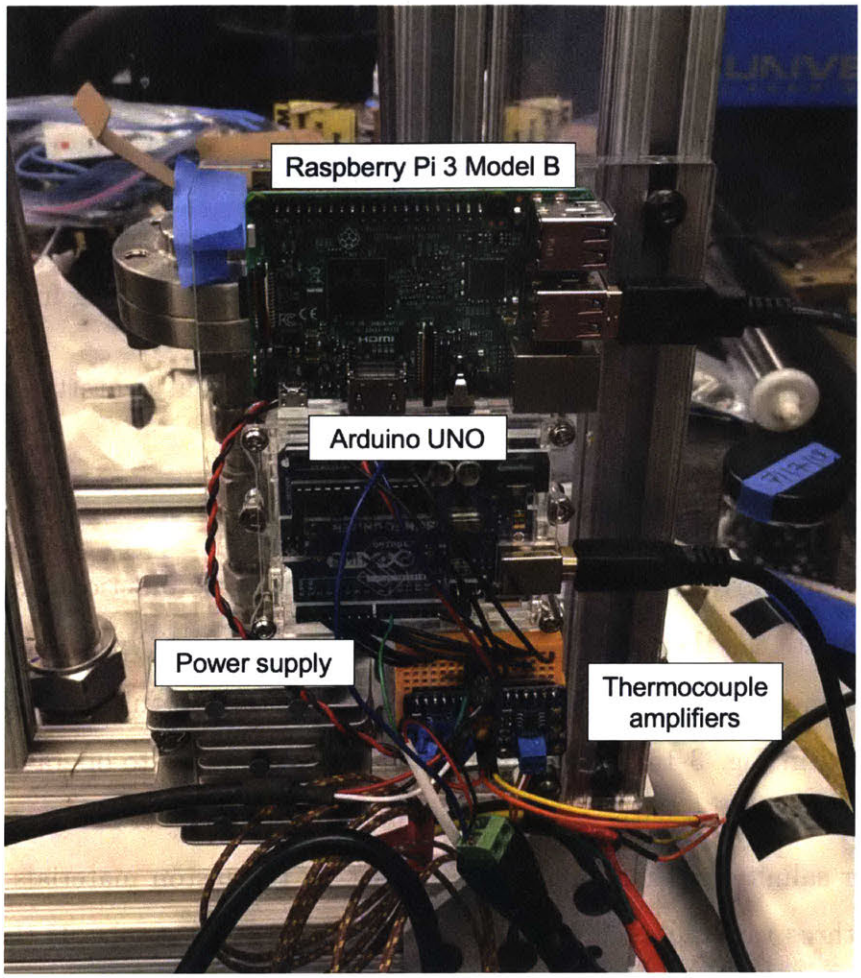

Figure 3-21: Main electronics control board for the HDRO prototype system. Not pictured here is the pressure transducer attached to the bottom of the piston.

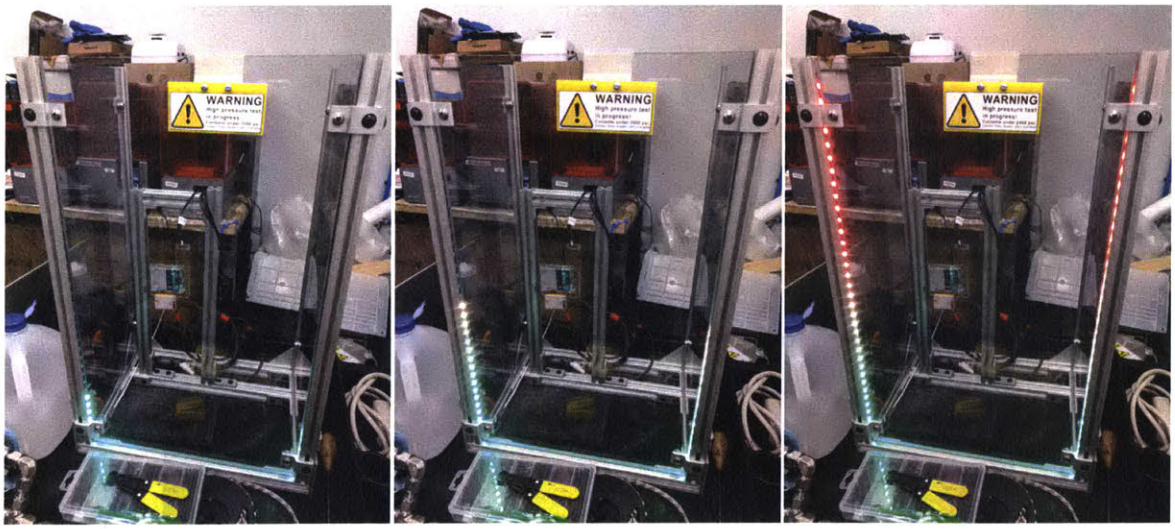

Figure 3-22: LEDs on the front of the protective case indicate the state of the pressure within the system. The height and color of the LEDs map to pressures ranging from 1-138 bar.

to the user. Admittedly, this feature is not entirely necessary but is pretty damn cool.

3.4.2 Experimental Procedure

The purpose of this early HDRO prototype is to test the basic functionality of the HDRO process and validate the thermodynamics analysis presented here. In particular, one major goal is to determine if the fuel efficiency and performance ratio of this system are within the bounds presented in Fig. 3-16. To accomplish this, it is necessary to operate this system at various recovery ratios and with various combinations of input fuel and water. For a fixed initial saltwater salinity and maximum pressure set by the piston materials and geometry, there are only three variables that can be varied for these experiments: 1) the initial height of the piston and consequently how much saltwater is initially added to the system, 2) the amount of fuel added to the top portion of the piston, and 3) the amount of reaction water added to the top portion of the piston.

To perform these experiments, the basic procedure outline in Fig. 3-23 is followed to set up and run the system. First, after installing the membrane in the membrane assembly, the piston is set to the height corresponding to the desired recovery ratio and output water yield. The test apparatus is then inverted such that the sediment trap below the membrane assembly is facing upwards. The cap on the sediment trap is removed and the lower portion

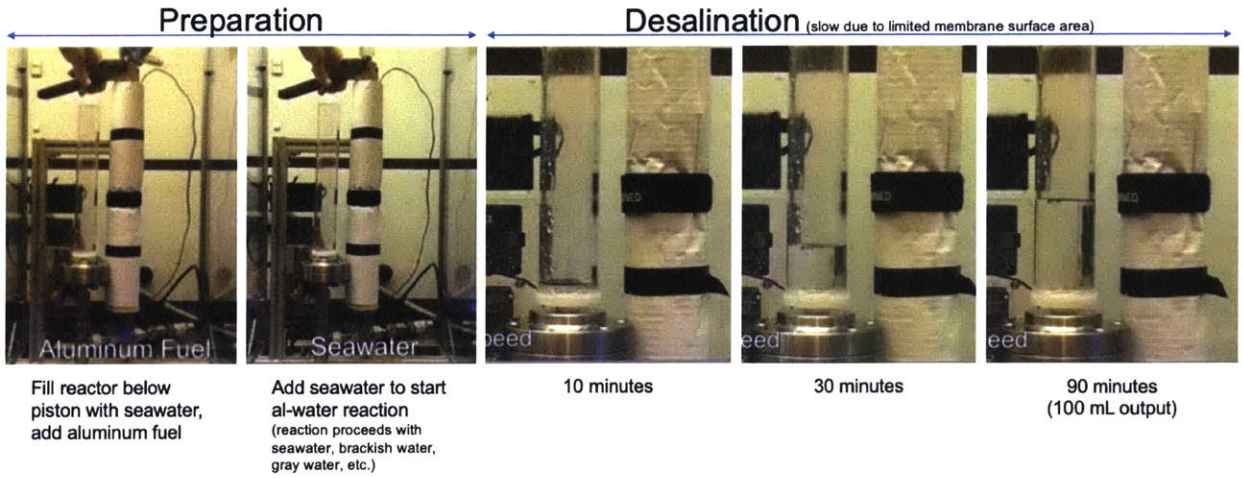

Figure 3-23: Typical process for running HDRO experiments.

of the prototype is filled with saltwater. It is crucial that the amount of water added in this step is precisely measured and recorded. Additionally, care is taken to add the water slowly to ensure that no pockets of air are trapped inside the piston or membrane assembly. Once filled, the sediment trap cap is replaced and tightened.

Before initiating the experiment, an additional step of precaution is taken to prevent combustion of the hydrogen inside the cylinder. Hydrogen has lower and upper explosive limits (i.e. the volume fractions of hydrogen in air between which an explosion can occur) 4% and 75% respectively [16]. At 138 bar, the volume fraction of hydrogen is well above the explosive limit; however, between 1 and 138 bar, the amount of hydrogen in the system briefly crosses into the explosive region. Furthermore, for experiments that do not go as intended, it is possible for the hydrogen production to stop before the upper limit is exceeded. To prevent this from happening, the top portion of the piston where the reaction occurs is initially flooded with inert argon gas. Because argon is more dense than air, as it settles into the piston, it displaces the air to fill the volume. With this added precaution, a hydrogen explosion is not possible as the oxidizer is removed from the system.

Once primed with argon, the desired mass of activated aluminum fuel and water for the reaction and generation of steam is added to the upper portion of the piston, and the top piston cap is quickly placed and wrench-tightened. An insulating fiberglass hood is placed over the top piston cap, and then the operator waits for data to be collected and recorded. This entire experiment is performed inside a fume hood.

Trial	Fuel Mass (g)	Reaction Water (mL)	Desal Output (mL)	Max Pressure (bar)	RR	PR
1*	3	15	23.2	60.2	0.29	1.38
2*	2.7	13	24.0	98.5	0.3	1.63
3	3.6	17.5	31	124	0.36	1.50
4	3.9	19	68.0	83.2	0.68	3.13
5	3.9	20	52.7	105	0.66	2.38

Table 3.3: Preliminary test trials. The trials marked with asterisk did not see complete reaction of the fuel input into the piston.

Finally, given the small volume of gas in the piston, the pressure is relieved after the system has had time to cool to room temperature simply by loosening the top cap slightly with a wrench to slowly bleed the gas from the system. Once it is confirmed that the system is depressurized, the contents of the piston are emptied and the experiment is reset for additional trials.

3.4.3 Initial Performance Results

The data collected for a typical performance trial is shown in Fig. 3-24, and includes the time-varying internal system pressure, the temperatures above and below the piston, and the volume of water desalinated. Immediately evident from these results is the significant difference in time scales for the desalination and aluminum-water reaction processes. In this particular example, the pressure reaches its maximum of roughly 117 bar within several minutes of beginning the trial while the desalination process reaches its final output after several hours. Qualitatively, these disparate time scales provide ample time for the thermal energy in the reactor to dissipate before the desalination is complete, regardless of how well insulated the piston is.

As expected, the results for these initial trials are on the low end of efficiency and on the high end of fuel consumption per unit volume desalinated. Table 3.3 summarizes the 5 trials performed for this initial prototype testing. For the first two tests it was observed that a majority of the fuel put into the piston did not react, as shown by an abundance of solid aluminum left over after the trials ended. These trials are therefore not included in the results provided here. For the experiments which resulted in complete fuel reactions,

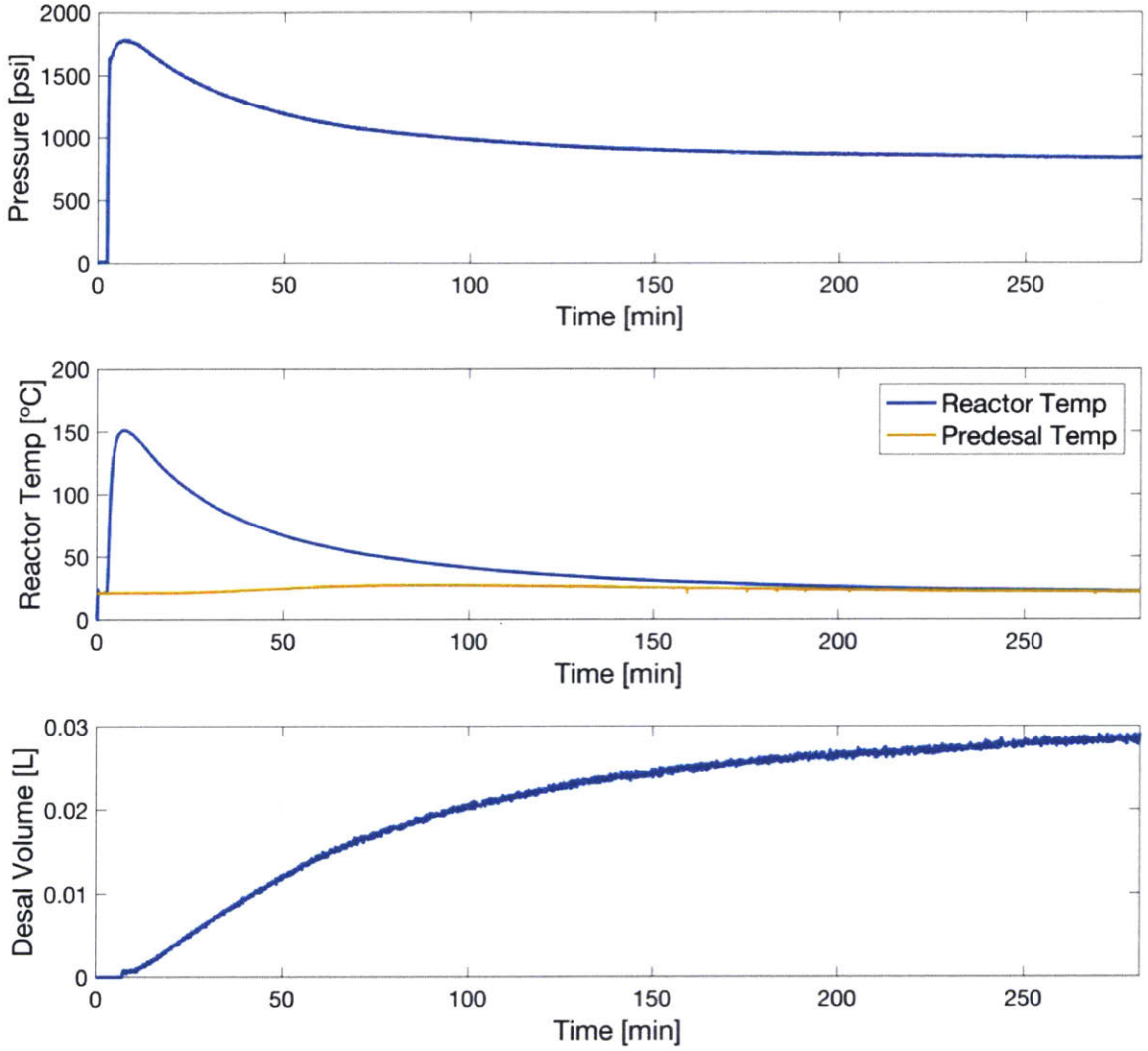

Figure 3-24: Typical data for an HDRO performance trial. The data shown here is for a recovery ratio of 0.65 operating at 120 g Al/L desalinated.

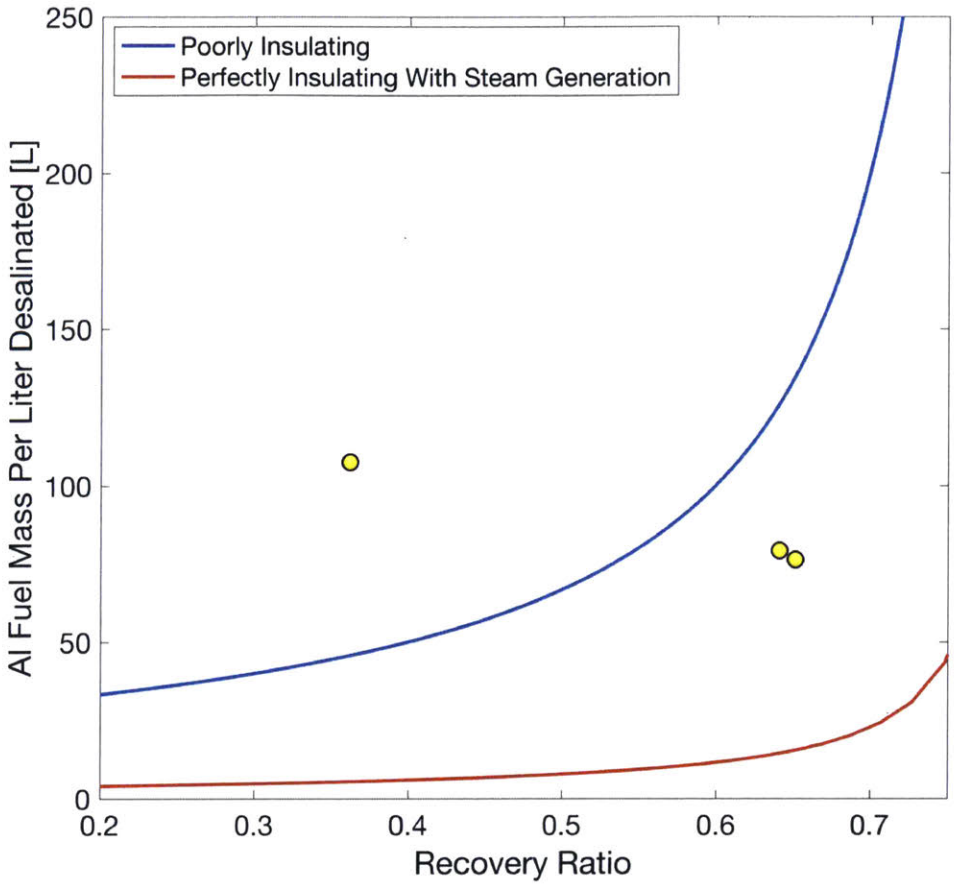

Figure 3-25: Fuel consumption results for initial HDRO prototype testing.

the fuel consumption and performance ratio for each trial are shown in Figs. 3-25 and 3-26 respectively.

As is shown here, the performance for two of the three trials were within the computed bounds on fuel consumption and efficiency. The major outlier in these trials is potentially the result of adding too much water to the reaction chamber or can otherwise be explained by reaction byproducts getting caught between the piston and the tube wall, increasing friction significantly. Future experiments at more carefully controlled recovery ratios will attempt to show the repeatability of this process and determine with more certainty whether the experimental results match the thermodynamics model presented here.

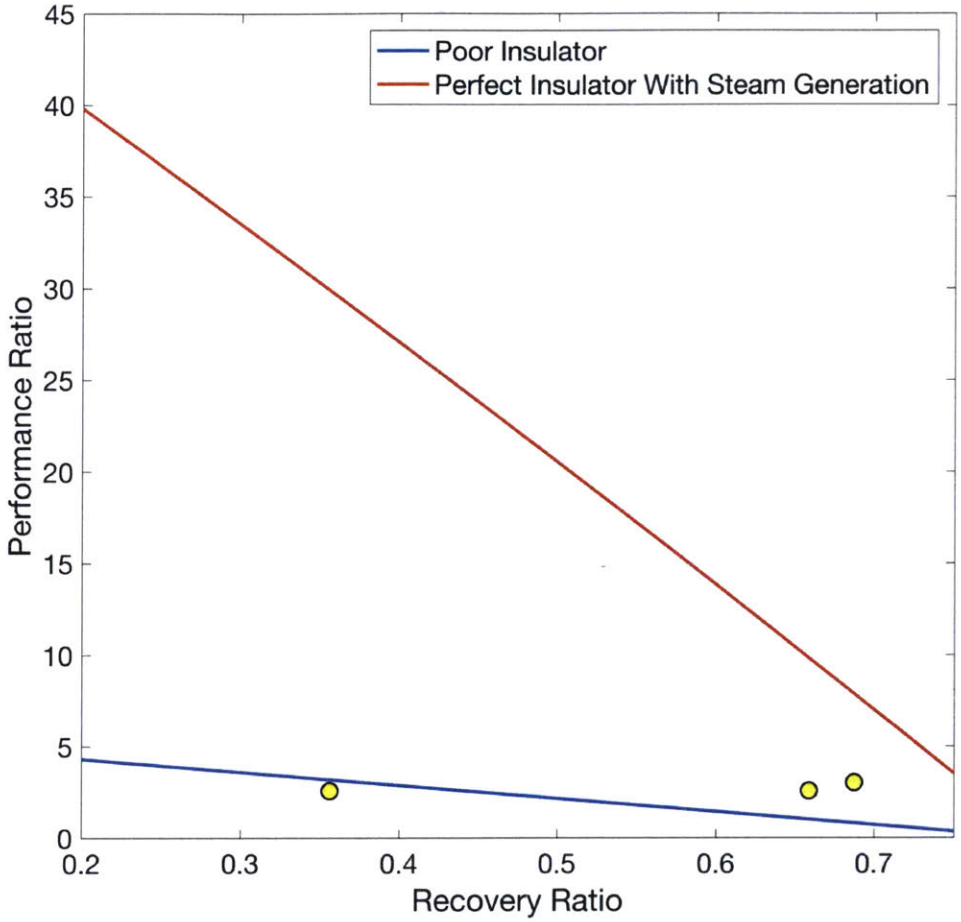

Figure 3-26: Performance ratio results for initial HDRO prototype testing.

3.4.4 Additional Sources of Error

There are numerous potential sources of error that can contribute to the experimental data not matching the thermodynamics analysis. First, regardless of how well insulated the outside of the piston is, in the prototype system, the reaction products inside the piston are exposed directly to the stainless steel tube. Consequently, some of the thermal energy released in the aluminum-water reaction is lost as sensible heat to the tube itself. In the energy balance shown in Eq. 3.22, this would show up as an added Δh for the mass of steel exposed to the reaction. Second, while the acetal piston is thermally insulating and acts slow the rate of heat being transferred between the reaction site and saltwater below it, there is still heat transfer that occurs through the steel tube and down into the water. In this configuration, the steel tube acts as a fin cooling the top portion of the piston. Finally, as previously mentioned, frictional losses in the piston and the membrane are ignored in this analysis, as well as any CP effects at the membrane surface. All of these factors must be incorporated into future iterations of the thermodynamics model in order for the experimental results to more closely align with the theoretical results.

3.5 Future Work

3.5.1 Improving Prototype Efficiency

Several key efficiency improvements are suggested here for future integration into this HDRO prototype. Improving the efficiency of the prototype will potentially enable more accurate testing of the upper efficiency bound analysis presented here and lay the initial groundwork for designing a more field-ready, practical system.

Better Thermal Insulation

As previously discussed, the primary sources of energy loss in this initial device implementation come from heat being transferred from the aluminum-water reaction products to the surrounding environment. A thicker or more thermally insulating material can be added to the outside of the piston to slow the rate of heat transfer along this path; however, a

significant issue is the transfer of thermal energy into the piston wall itself, which is not mitigated by better external insulation. It is therefore suggested that an additional insulating material be placed in between the reaction site and the inner wall of the piston tube. Care must be taken, however, to ensure that the insulating material can both withstand the expected system temperature and that the material is ductile enough to withstand flexing slightly as the high system pressure pushes it against the piston wall. Ceramics, for example, can withstand extreme temperatures but may be too brittle to be used for this application. Alternatively, common thermoplastics have the reverse issue whereby they are highly ductile but cannot withstand the 200-400 °C temperatures expected for this system, especially when operating at low recovery ratios. More expensive and exotic plastics and ceramics do exist, however, that strike a better balance between these two material properties and should be considered in the next prototype iteration. Thermoplastics like Vespel® and Torlon®, for example, can withstand temperatures up to 300 °C, and while expensive, they would suffice for improving the efficiency for experimental purposes only.

A simpler, though less effective mitigation strategy would be to place a short ceramic cylinder inside the top portion of the piston that can ride along with the piston as water is desalinated. Because this inner cylinder would be open at the top, there would not be a pressure drop across its wall, and thus no special mechanical properties would be required. As the reaction proceeds, the ceramic would act to insulate the reaction products from the piston wall as intended. The main limitation here, however, would be that as the piston moves down to force more water through the membrane, the inner ceramic cylinder would follow the piston, exposing more and more of the piston wall above it to the product gasses. For low recovery ratios, this may be an acceptable solution and should be explored in further detail.

Slower Rate of Reaction

While thermal energy losses are due in large part to the construction of the prototype itself, they are also a function of the disparate reaction and desalination timescales, as all physical systems are poor insulators if given enough time for the thermal energy to dissipate. For this system, it is potentially desirable to react aluminum and water at a slower rate to

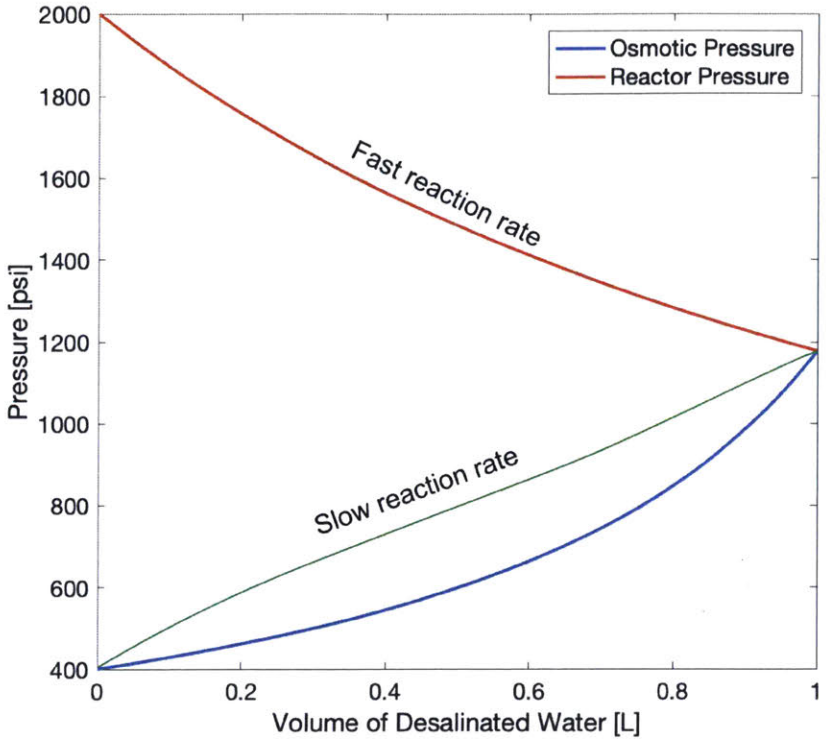

Figure 3-27: Comparison of different aluminum-water reaction rates in an HDRO system.

more optimally stage the release of thermal energy. Fig. 3-27, shows the system pressures that evolve as more water is desalinated for two reaction rate scenarios. The orange (top) curve reflects the comparatively fast reaction rate of the current prototype, which causes the internal pressure to spike initially to a value that is much higher than the osmotic pressure (bottom, blue curve). This pressure then drops as the piston expands until it hits the osmotic pressure and the process finishes. Alternatively, the green (middle) curve in this figure reflects a slower reaction rate that results in the production of hydrogen and release of thermal energy such that the internal pressure is always only slightly above the osmotic pressure throughout the entire process. Inherently, there is some trade-off here as the higher the overpressure, the greater the rate of desalination. A slower reaction rate therefore means that the desalination process takes longer, reducing its potential advantage. Further analysis should be performed to determine the optimal rate of reaction for this type of approach.

If it is determined that there is some optimal slower reaction rate that could effectively combat this difference in timescales, there are two main strategies for accomplishing this

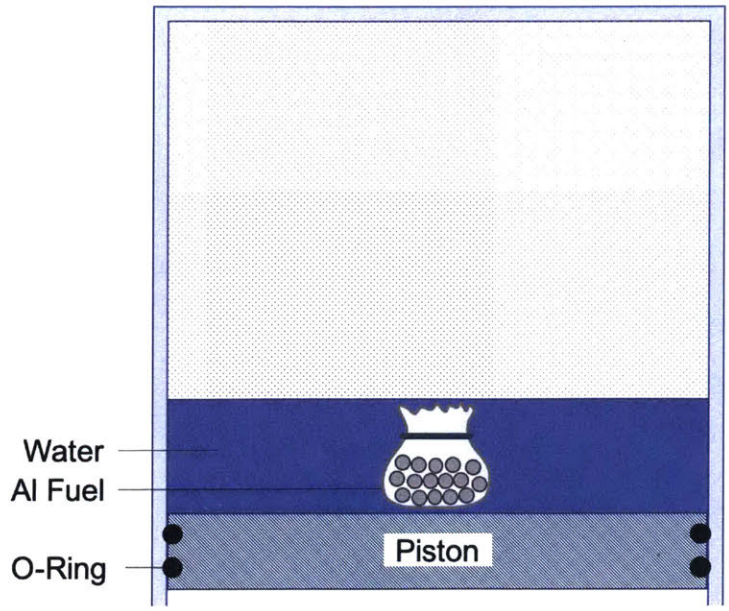

Figure 3-28: Potential method for slowing the aluminum-water reaction rate by inhibiting the flux of water to the fuel itself.

to explore here. Note that given the desire to keep this system as simple and robust as possible for disaster relief applications, only passive approaches are considered here. First, as illustrated in Fig. 3-28, the fuel can be placed in an expandable water-wicking secondary container (i.e. sock) that reduces the flux of water to the reaction site. By choosing different sock materials of varying densities, this flux can be tuned to achieve a range of slower reaction rates. Second, it has been observed that the reaction of aluminum with saltwater exhibits similar hydrogen yields but at much lower reaction rates. While yet to be explored in detail, changing the salinity of the reaction water may be an effective method for slowing the reaction rate in a predictable manner.

Increased Desalination Rate

The other obvious approach to reducing the difference in timescales between the aluminum-water reaction and the desalination process is to increase permeation rate of water through the membrane. This can be accomplished by either operating the system at higher pressures or increasing the surface area of the membrane. Given that this system is already designed to operate at the maximum pressure that can safely be achieved for the piston material and

geometry, the only way to increase this parameter is to use more expensive materials or thicker-walled tubing, both of which may contribute significantly to capital costs and overall system weight. Far cheaper and simpler would be to increase the membrane area, using rolled membrane assemblies typically seen in commercial RO plants. These assemblies are typically designed for lower system pressure and for continuous flow operation but can be easily modified to work with the HDRO prototype presented here. In the current implementation, the membrane used is a small 47 mm diameter disk, so as it stands, there is significant room for improvement here.

3.5.2 Thermodynamics Model Improvements

To better understand how the experimental data deviates from the ideal thermodynamics model presented here, it will be necessary to model the actual prototype system as accurately as possible. In addition to including the aforementioned frictional losses from both the piston and the pressure drop across the membrane, it will also be necessary to develop a model that takes into account additional transient effects like thermal dissipation and concentration polarization, which is a function of the permeation rate of water through the membrane. This new analysis would also need to model the kinetics of the aluminum-water reaction itself to most effectively understand how the heat release might be able to be staged more optimally over the course of the desalination process. In general, as previously described in detail, there are numerous trade-offs to be made when operating at different recovery ratios, and many of these are not captured in the original analysis presented here. The proposed transient models that include the thermophysical properties of actual system components will enable more realistic efficiency optimization and performance characterization.

3.5.3 Utility Scale HDRO

Despite being on the lower end of the efficiency bounds predicted for the HDRO process, the results are promising enough to warrant investigation into how the system might scale to be able to provide water to drought-prone towns or cities with ample access to waste heat or aluminum debris. Given that the performance ratio for this process is potentially

significantly higher than that for MED and MSF, it is worthwhile to understand what range of capital and operating costs can be expected for an HDRO plant at this larger scale. Additional logistical and process-related functions will need to be analyzed as well, including fuel production, waste management, eutectic recovery, and electricity production from the generated hydrogen produced, in order to understand the full technoeconomics behind this desalination approach and determine both whether or not it is feasible and on what scale.

3.5.4 HDRO Using Other Sources of Thermal Energy

Solar Thermal

The analysis presented here was performed assuming an aluminum-water reaction is used to supply the thermal energy required to drive HDRO. In general, however, HDRO is introduced here as a method for using any acceptable thermal energy source to drive RO desalination. Using a system shown in Fig. 3-29, solar thermal energy, for example, can be absorbed into the piston walls to heat a two phase ammonia solution. The vapor pressure of this solution at the temperature that results from the system being exposed to direct sunlight can be tuned to be well above the osmotic pressure of the saltwater below the piston by altering the composition of the ammonia solution. At night or out of direct sunlight, the vapor pressure should be sufficiently low such that the system can be reset to desalinate more saltwater. An added benefit of this type of HDRO implementation is that the working fluid can remain enclosed in the piston for the entire life of the device. No waste management is required, as the system can be reset simply by returning the piston to its starting position once the ambient temperature is sufficiently low.

For desalination at night or at times when sunlight is unavailable, solar thermal energy can be stored in the phase change of materials like sodium nitrate, which melt at high temperatures. These materials can be exposed to the top portion of the piston in order to supply the thermal energy needed to generate the high pressures required for HDRO. As previously shown, with a well insulated system, the performance of this type of heat source should be similar to that of the aluminum-water reaction, as the production of hydrogen only contributes a small amount to the maximum system pressure achieved during the HDRO

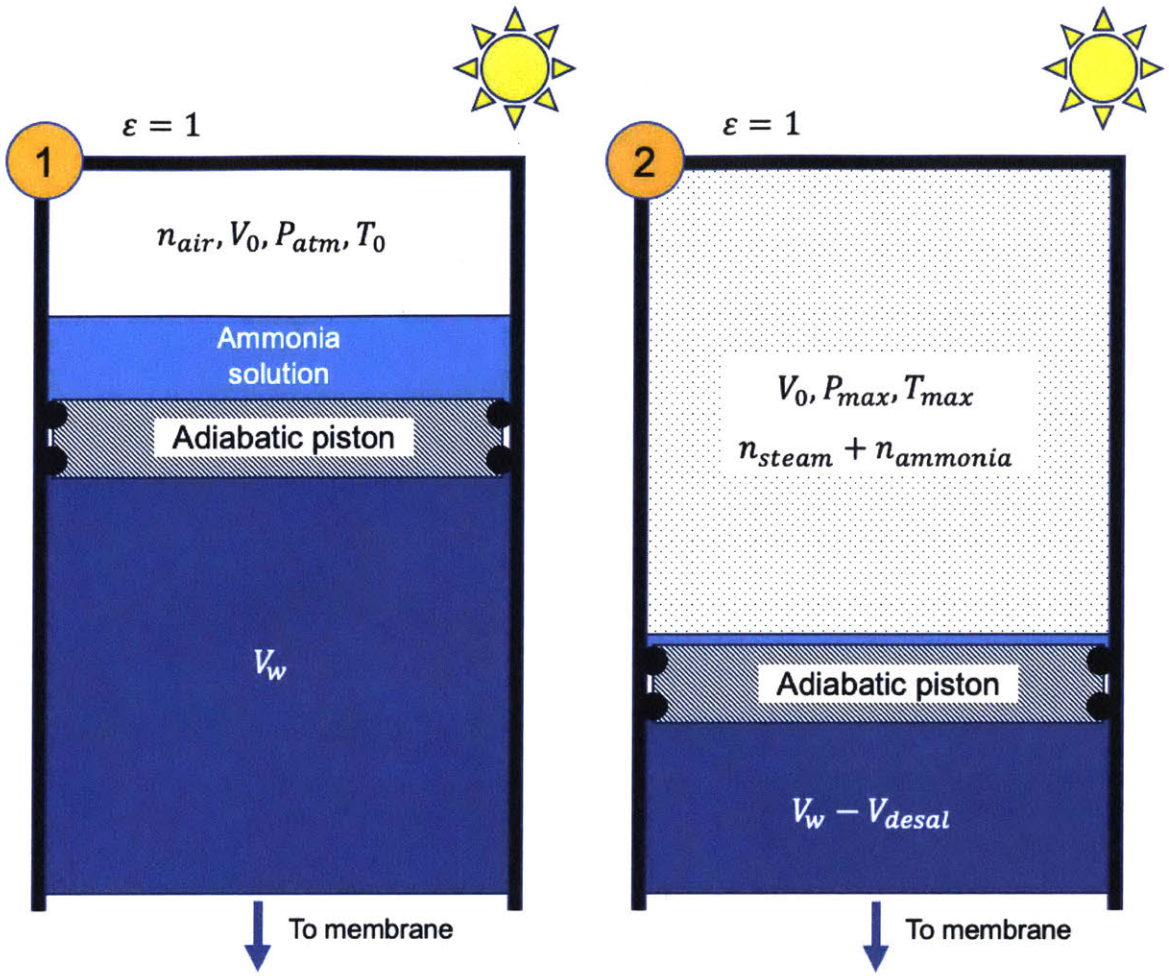

Figure 3-29: Concept model for using solar thermal energy to drive HDRO. Here ammonia solution with a carefully tuned vapor pressure profile acts as working fluid in this process.

process. Thus, this total solar-thermal HDRO approach has the potential to significantly improve the capacity factor of solar-driven desalination, enabling it to become more feasible for medium scale disaster relief applications.

Cogeneration

Another common source of waste heat is from power plants that burn natural gas or other fossil fuels to generate work via Brayton or Rankine cycles. The combustion products at the outlet of the turbine in a Brayton cycle, for example, can be as high as 700 °C[1]. Typically, this exhausted thermal energy is either used to preheat air or fuel going into the combustion chamber or is used in a cogeneration configuration, in which the thermal energy generates hot

water or steam to supply a district heating system. For smaller plants or backup generators, it is not economical to run a cogeneration loop, and thus this heat is often vented to the environment. For these applications, especially for emergency generators, an HDRO system may be coupled with this thermal energy source to power desalination highly efficiently at the scale considered in this research. Future work should be conducted to determine the optimal configuration for this type of approach and on what scales it is feasible.

Chapter 4

Conclusion

The work presented in this thesis contributes fundamentally to the ability to take aluminum debris, convert it a fuel that reacts with water to produce hydrogen and heat, use the hydrogen to generate electricity, and use that heat to desalinate or purify water, in particular for applications related to disaster relief and resiliency. As climate change continues to create the conditions necessary for more frequent and potent natural disasters like hurricanes, wildfires, and droughts to occur, there is an ever increasing need for these types of technologies that can deliver energy-dense and robust solutions for generating electricity and potable water in the aftermath of these disasters.

To this end, a new experimentally validated thermodynamics model of aluminum-water reactions is first presented that enables a more accurate understanding of how these reactions can be used to generate hydrogen and heat. This reaction is analyzed over temperatures and pressures ranging from 273.15-600 K and 0.1-10 MPa respectively. Over this range, aluminum and water can react to form a number of different aluminum oxide and hydroxide species, each of which alters the amount of thermal energy released and how much water is required stoichiometrically for the reaction to proceed, both crucial parameters for developing applications that use aluminum as a fuel. The new model presented here uses the Gibbs free energy to predict the favorability of each of these possible reactions as a function of temperature and pressure, and these results were validated by running reactions at the extremities of the operating range and analyzing the byproduct composition using FTIR and XRD methods. The experimental results were in close alignment with the model. Addition-

ally, reaction tests above 423 K and at 0.1 MPa indicate limited reactivity between steam and aluminum activated using the methods presented here. Consequently, the thermodynamics model is modified to show that the aluminum oxide byproduct cannot be achieved in practice using this method as its transition remains above the saturation curve for water.

Second, a novel and highly efficient method for using thermal energy to drive reverse osmosis desalination is presented here as means for using the heat released in the aluminum-water reaction to desalinate seawater. This method, called Heat-Driven Reverse Osmosis (HDRO), uses this heat to generate high pressures in an enclosed, thermally insulated piston that in turn push saltwater against a semipermeable membrane, allowing only pure water to permeate through. A thermodynamics analysis is developed to theoretically bound the fuel efficiencies and total system volume for such a device, indicating that for low recovery ratios, HDRO can operate up to 41 times more efficiently than single stage evaporative desalination processes, making it potentially competitive with state-of-the-art MED and MSF processes as well. This HDRO process is tested experimentally using an unoptimized prototype system, and preliminary results show this device performing at least three times more efficiently than simply boiling off the equivalent quantity of water. Follow on work is outlined for making this prototype more efficient and for enabling the use of different sources of heat, including solar thermal, that can be used to power disaster-relief scale desalination efficiently.

Throughout the world, in developed and developing nations alike, communities are struggling with an ever-increasing influx of aluminum waste, while simultaneously grappling with depleted or rapidly dwindling clean water supplies. In the US, billions of kilograms of aluminum are recycled each year, but in most regions nearly half of this aluminum still winds up unused in landfills. All the while, states on the West Coast are highly susceptible to drought. In places like Puerto Rico, for example, recycling programs are non-existent, causing landfills to overflow with aluminum waste. To compound this issue, Puerto Rico and its neighboring islands are also highly susceptible to hurricanes and other natural disasters that cause widespread damage to cars and homes, and in the aftermath of these disasters, there is a high influx of scrap aluminum, which can overburden an already insufficient waste management program. One can therefore imagine a complete ecosystem in which people are provided with a means of extracting the energy from the aluminum waste to power seawater

desalination, generate electricity, and sell the aluminum oxyhydroxide byproduct to cover operational costs. Used in this way, the technology developed and shown here has the potential to add resiliency to communities' water and electricity infrastructure, as well as improve disaster preparedness for those in natural-disaster prone regions. Ultimately, this and follow on work may encourage these communities to to divert aluminum destined for scrap yards and landfills into theses processes that can generate valuable and critical resources locally.

Appendix A

Computed Gibbs Free Energy Values

The change in Gibbs free energy for each of the three aluminum-water reactions given by Eq. 2.1-2.3 are shown in Tables A- A.3 respectively across the temperature and pressure ranges considered in this research. Note for each of these tables, the values presented are per two moles of aluminum, as shown in these equations.

	p [MPa]									
T [°C]	0.1	1.1	2.1	3.1	4.1	5.1	6.1	7.1	8.1	9.1
0	-886.4	-876.1	-877.6	-880.9	-884.9	-889.3	-894.0	-898.9	-903.9	-909.0
25	-887.7	-875.8	-876.9	-880.0	-883.8	-888.1	-892.7	-897.4	-902.4	-907.4
50	-888.6	-875.3	-876.0	-878.7	-882.4	-886.6	-891.0	-895.7	-900.6	-905.6
75	-889.2	-874.4	-874.7	-877.2	-880.7	-884.8	-889.1	-893.7	-898.5	-903.4
100	-889.6	-873.3	-873.2	-875.5	-878.8	-882.7	-886.9	-891.4	-896.1	-900.9
125	-889.6	-871.8	-871.3	-873.4	-876.5	-880.3	-884.4	-888.8	-893.4	-898.2
150	-889.3	-870.1	-869.2	-871.0	-873.9	-877.6	-881.6	-885.9	-890.4	-895.1
175	-888.8	-868.0	-866.7	-868.3	-871.1	-874.6	-878.5	-882.7	-887.1	-891.7
200	-888.0	-865.7	-864.0	-865.3	-867.9	-871.3	-875.1	-879.2	-883.6	-888.1
225	-886.8	-863.1	-861.0	-862.1	-864.5	-867.7	-871.4	-875.4	-879.7	-884.2
250	-885.4	-860.2	-857.6	-858.5	-860.8	-863.8	-867.4	-871.3	-875.5	-879.9
275	-883.7	-856.9	-854.0	-854.6	-856.7	-859.6	-863.1	-866.9	-871.1	-875.4
300	-881.6	-853.4	-850.1	-850.5	-852.4	-855.2	-858.5	-862.3	-866.3	-870.6

Table A.1: $\Delta G_{rxn}(T, p)$ [kJ/mol] for the shown in Eq. 2.1, producing $Al(OH)_3$.

	p [MPa]									
T [°C]	0.1	1.1	2.1	3.1	4.1	5.1	6.1	7.1	8.1	9.1
0	-885.0	-872.9	-872.5	-874.0	-876.1	-878.7	-881.6	-884.6	-887.8	-891.1
25	-888.2	-874.6	-873.8	-875.0	-877.0	-879.5	-882.2	-885.2	-888.3	-891.5
50	-891.2	-876.1	-874.9	-875.9	-877.7	-880.0	-882.6	-885.5	-888.5	-891.6
75	-894.0	-877.3	-875.8	-876.5	-878.1	-880.3	-882.8	-885.6	-888.5	-891.6
100	-896.5	-878.4	-876.5	-876.9	-878.4	-880.4	-882.9	-885.5	-888.4	-891.4
125	-898.9	-879.3	-876.9	-877.1	-878.4	-880.3	-882.6	-885.2	-888.0	-890.9
150	-901.0	-879.9	-877.2	-877.1	-878.3	-880.0	-882.2	-884.7	-887.4	-890.2
175	-903.0	-880.4	-877.2	-876.9	-877.9	-879.5	-881.6	-884.0	-886.6	-889.4
200	-904.7	-880.6	-877.0	-876.5	-877.3	-878.8	-880.8	-883.1	-885.6	-888.3
225	-906.2	-880.6	-876.7	-875.9	-876.5	-877.9	-879.7	-881.9	-884.4	-887.0
250	-907.5	-880.4	-876.1	-875.1	-875.5	-876.7	-878.5	-880.6	-882.9	-885.5
275	-908.6	-880.0	-875.3	-874.0	-874.3	-875.4	-877.0	-879.0	-881.3	-883.8
300	-909.5	-879.4	-874.3	-872.8	-872.9	-873.8	-875.3	-877.2	-879.4	-881.9

Table A.2: $\Delta G_{rxn}(T, p)$ [kJ/mol] for the shown in Eq. 2.2, producing $AlOOH$.

	p [MPa]									
T [°C]	0.1	1.1	2.1	3.1	4.1	5.1	6.1	7.1	8.1	9.1
0	-866.4	-853.6	-852.7	-853.5	-855.1	-857.1	-859.4	-861.8	-864.4	-867.1
25	-870.8	-856.5	-855.2	-855.8	-857.2	-859.1	-861.2	-863.6	-866.1	-868.7
50	-875.0	-859.3	-857.6	-857.9	-859.2	-860.9	-862.9	-865.2	-867.6	-870.2
75	-879.1	-861.9	-859.8	-859.9	-860.9	-862.5	-864.5	-866.6	-869.0	-871.5
100	-883.1	-864.4	-861.8	-861.7	-862.6	-864.0	-865.9	-867.9	-870.2	-872.6
125	-886.9	-866.7	-863.7	-863.4	-864.1	-865.4	-867.1	-869.1	-871.3	-873.6
150	-890.5	-868.8	-865.5	-864.9	-865.4	-866.6	-868.2	-870.1	-872.2	-874.4
175	-894.0	-870.8	-867.1	-866.2	-866.6	-867.6	-869.1	-870.9	-872.9	-875.1
200	-897.3	-872.6	-868.5	-867.4	-867.6	-868.5	-869.9	-871.6	-873.5	-875.6
225	-900.5	-874.3	-869.8	-868.4	-868.4	-869.2	-870.5	-872.1	-873.9	-876.0
250	-903.5	-875.9	-870.9	-869.3	-869.2	-869.8	-870.9	-872.5	-874.2	-876.2
275	-906.4	-877.2	-871.9	-870.0	-869.7	-870.2	-871.3	-872.7	-874.4	-876.2
300	-909.1	-878.4	-872.7	-870.6	-870.1	-870.5	-871.4	-872.7	-874.3	-876.2

Table A.3: $\Delta G_{rxn}(T, p)$ [kJ/mol] for the reaction shown in Eq. 2.3, producing Al_2O_3.

Bibliography

[1] M.A. Alabdoadaim, B. Agnew, and I. Potts. "Performance analysis of combined Brayton and inverse Brayton cycles and developed configurations". In: *Applied Thermal Engineering* 26.14-15 (Oct. 2006), pp. 1448–1454. ISSN: 1359-4311. DOI: 10.1016/J.APPLTHERMALENG.2006.01.003. URL: https://www.sciencedirect.com/science/article/pii/S1359431106000111.

[2] Babak Alinejad and Korosh Mahmoodi. "A novel method for generating hydrogen by hydrolysis of highly activated aluminum nanoparticles in pure water". In: *International Journal of Hydrogen Energy* 34.19 (Oct. 2009), pp. 7934–7938. ISSN: 0360-3199. DOI: 10.1016/J.IJHYDENE.2009.07.028. URL: https://www.sciencedirect.com/science/article/pii/S036031990901091X.

[3] Craig P Aubuchon and Kevin M Morley. "The Economic Value of Water: Providing Confidence and Context to FEMA's Methodology". In: *Homeland Security & Emergency Management* 10.1 (2013), pp. 245–265. DOI: 10.1515/jhsem-2012-0081. URL: http://online.wsj.com/article/SB10001424052970204831304576594872744l0.

[4] O. C. Bridgeman and E. W. Aldrich. "Vapor Pressure Tables for Water". In: *Journal of Heat Transfer* 86.2 (1964), p. 279. ISSN: 00221481. DOI: 10.1115/1.3687121. URL: http://HeatTransfer.asmedigitalcollection.asme.org/article.aspx?articleid=1433184.

[5] E. David and J. Kopac. "Hydrolysis of aluminum dross material to achieve zero hazardous waste". In: *Journal of Hazardous Materials* 209-210 (Mar. 2012), pp. 501–509. ISSN: 0304-3894. DOI: 10.1016/J.JHAZMAT.2012.01.064. URL: https://www.sciencedirect.com/science/article/pii/S0304389412000957.

[6] *Global Share of Primary and Recycled Metal Production.* URL: http://recycling.world-aluminium.org/review/recycling-indicators/.

[7] Peter Godart et al. "Hydrogen production from aluminum-water reactions subject to varied pressures and temperatures". In: *International Journal of Hydrogen Energy* (Apr. 2019). ISSN: 0360-3199. DOI: 10.1016/J.IJHYDENE.2019.03.140. URL: https://www.sciencedirect.com/science/article/pii/S0360319919311486.

[8] B.S. Hemingway, R.A. Robie, and J.A. Apps. "Revised values for the thermodynamic properties of boehmite, AlO(OH) , and related species and phases in the system Al-H-O". In: *American Mineralogist* 76.3-4 (1991), pp. 445–457. URL: https://pubs.er.usgs.gov/publication/70016664.

[9] Eric M.V. Hoek et al. "Modeling the effects of fouling on full-scale reverse osmosis processes". In: *Journal of Membrane Science* 314.1-2 (Apr. 2008), pp. 33–49. ISSN: 0376-7388. DOI: 10.1016/J.MEMSCI.2008.01.025. URL: https://www.sciencedirect.com/science/article/pii/S0376738808000586.

[10] A.V. Ilyukhina, A.S. Ilyukhin, and E.I. Shkolnikov. "Hydrogen generation from water by means of activated aluminum". In: *International Journal of Hydrogen Energy* 37.21 (Nov. 2012), pp. 16382–16387. DOI: 10.1016/J.IJHYDENE.2012.02.175. URL: https://www.sciencedirect.com/science/article/pii/S036031991200540X.

[11] A.V. Ilyukhina et al. "Mechanochemical activation of aluminum with gallams for hydrogen evolution from water". In: *International Journal of Hydrogen Energy* 35.5 (Mar. 2010), pp. 1905–1910. ISSN: 0360-3199. DOI: 10.1016/J.IJHYDENE.2009.12.118. URL: https://www.sciencedirect.com/science/article/pii/S0360319909020461.

[12] Soorya Kabekkodu. *ICDD (2019). PDF-4+ 2019 (Database).* 2019.

[13] S Kalpakjian, SR Schmid, and H Musa. *Manufacturing engineering and technology: machining.* 2011.

[14] J. T. Kloprogge, H. D. Ruan, and R. L. Frost. "Thermal decomposition of bauxite minerals: infrared emission spectroscopy of gibbsite, boehmite and diaspore". In: *Journal of Materials Science* 37.6 (2002), pp. 1121–1129. ISSN: 00222461. DOI: 10.1023/A:1014303119055. URL: http://link.springer.com/10.1023/A:1014303119055.

[15] Chia-Tsun Liu and William T. Lindsay. "Vapor pressure of deuterated water from 106 to 300.deg." In: *Journal of Chemical & Engineering Data* 15.4 (Oct. 1970), pp. 510–513. ISSN: 0021-9568. DOI: 10.1021/je60047a015. URL: http://pubs.acs.org/doi/abs/10.1021/je60047a015.

[16] *Lower and Upper Explosive Limits for Flammable Gases and Vapors (LEL/UEL).* URL: https://www.mathesongas.com/pdfs/products/Lower-(LEL)-&-Upper-(UEL)-Explosive-Limits-.pdf.

[17] Bonnie J. McBride, Michael J. Zehe, and Sanford Gordon. *NASA Glenn Coefficients for Calculating Thermodynamic Properties of Individual Species.* Tech. rep. NASA Glenn Research Center, Sept. 2002. URL: https://ntrs.nasa.gov/search.jsp?R=20020085330.

[18] Wojciech Z. Misiolek et al. "High quality extrudates from aluminum chips by new billet compaction and deformation routes". In: *CIRP Annals* 61.1 (Jan. 2012), pp. 239–242. ISSN: 0007-8506. DOI: 10.1016/J.CIRP.2012.03.113. URL: https://www.sciencedirect.com/science/article/pii/S0007850612001151.

[19] Karan Mistry et al. "Generalized Least Energy of Separation for Desalination and Other Chemical Separation Processes". In: *Entropy* 15.12 (May 2013), pp. 2046–2080. ISSN: 1099-4300. DOI: 10.3390/e15062046. URL: http://www.mdpi.com/1099-4300/15/6/2046.

[20] O.J. Morin. "Design and operating comparison of MSF and MED systems". In: *Desalination* 93.1-3 (Aug. 1993), pp. 69–109. ISSN: 0011-9164. DOI: 10.1016/0011-9164(93)80097-7. URL: https://www.sciencedirect.com/science/article/pii/0011916493800977.

[21] John Petrovic and George Thomas. *Reaction of Aluminum with Water to Produce Hydrogen.* Tech. rep. Office of Energy Efficiency and Renewable Energy (EERE), Washington, DC, 2010.

[22] *Puerto Rico Contractor Begins Recycling Excess Water Bottles.* 2018. URL: https://www.fema.gov/news-release/2018/12/06/puerto-rico-contractor-begins-recycling-excess-water-bottles.

[23] SS Sablani et al. "Concentration polarization in ultrafiltration and reverse osmosis: a critical review". In: *Desalination* 141.3 (Dec. 2001), pp. 269–289. ISSN: 0011-9164. DOI: 10.1016/S0011-9164(01)85005-0. URL: https://www.sciencedirect.com/science/article/pii/S0011916401850050.

[24] JoséM. Saniger. "Al-O infrared vibrational frequencies of γ-alumina". In: *Materials Letters* 22.1-2 (Jan. 1995), pp. 109–113. ISSN: 0167-577X. DOI: 10.1016/0167-577X(94)00234-7. URL: https://www.sciencedirect.com/science/article/pii/0167577X94002347.

[25] Kelsey C Seto. "Hydrogen production from aluminum-water reactions subject to high pressure and temperature conditions". In: (2017). URL: https://dspace.mit.edu/handle/1721.1/111936?show=full.

[26] Fink Sheri. *Puerto Rico: How Do We Know 3,000 People Died as a Result of Hurricane Maria? - The New York Times.* 2018. URL: https://www.nytimes.com/2018/06/02/us/puerto-rico-death-tolls.html.

[27] Vladimir Shmelev, Heesung Yang, and Chungsik Yim. "Hydrogen generation by reaction of molten aluminum with water steam". In: *International Journal of Hydrogen Energy* 41.33 (Sept. 2016), pp. 14562–14572. ISSN: 0360-3199. DOI: 10.1016/J.IJHYDENE.2016.05.277. URL: https://www.sciencedirect.com/science/article/pii/S0360319916317694.

[28] Jonathan Slocum. *Activated aluminum fuel.* June 2016. URL: https://patents.google.com/patent/US20160355918A1/en.

[29] Jonathan Thurston Slocum. "Characterization and science of an aluminum fuel treatment process". In: (2017). URL: https://dspace.mit.edu/handle/1721.1/115674.

[30] *Statistics Progress in Puerto Rico, Hurricane Maria Update.* URL: https://www.fema.gov/media-library/assets/images/151463.

[31] W Vedder and D A Vermilyea. "Aluminum + Water Reaction". In: *Trans. Faraday Soc.* 65 (1969), pp. 561–584. DOI: 10.1039/TF9696500561.

[32] Jeffrey T. Ziebarth et al. "Liquid phase-enabled reaction of Al–Ga and Al–Ga–In–Sn alloys with water". In: *International Journal of Hydrogen Energy* 36.9 (May 2011), pp. 5271–5279. ISSN: 0360-3199. DOI: 10.1016/J.IJHYDENE.2011.01.127. URL: https://www.sciencedirect.com/science/article/pii/S0360319911002175.